



C.J. Deacon  
Manager, Advanced Reactor Programs

General Electric Company  
175 Curtner Avenue, M/C 365 San Jose, CA 95125-1014  
408 925-2469 (phone) 408 925-5474 (facsimile)

MFN 02-098

Project 717

December 20, 2002

U.S. Nuclear Regulatory Commission  
ATTN: Document Control Desk  
One White Flint North  
11555 Rockville Pike  
Rockville, MD 20852-2738

Attention: Chief, Information Management Branch  
Program Management  
Policy Development and Analysis Staff

Reference: Letter S. Hucik, GE to S. Collins, NRC, Pre-application Review of ESBWR,  
dated April 18, 2002

Subject: **TRACG Qualification for ESBWR, NEDC-33080 - Document Transmittal  
for Pre-Application Review of ESBWR**

The CD accompanying this letter contains the GE non-proprietary report TRACG Qualification for ESBWR, NEDC-33080. It is item number 6 in Enclosure 1. This report is submitted in support of the pre-application review of the ESBWR (Reference).

GE is seeking approval for the use of the TRACG code for the one-time application for Design Certification of the ESBWR. The report NEDC-33080, represents one of several reports that support the NRC review of TRACG for this application. The ESBWR Design Description, NEDC-33084 (Item 1, Enclosure 1) provides a description of the reference ESBWR design. The ESBWR Test and Analysis Program Description (TAPD), NEDC-33079, (Item 2, Enclosure 1) defines the necessary qualification program for the ESBWR. The TRACG Model Description, NEDE-32176P, (Item 3, Enclosure 1) was submitted to the staff in December 1999. The overall qualification of TRACG for the ESBWR consists of three parts. TRACG Qualification, NEDE-32177P (Item 4, Enclosure 1) was submitted in January 2000. TRACG Qualification for SBWR, NEDC-32725P (Item 5, Enclosure 1) and the companion TRACG Qualification for ESBWR, NEDC-33080, (Item 6, Enclosure 1), complete the TRACG qualification basis for ESBWR. The report TRACG Application for Anticipated Operational Occurrences Transient Analyses, NEDE-32906P (Item 11, Enclosure 1) forms the basis for application to Anticipated Operational Occurrences (AOOs) for the ESBWR.

GE intends to follow a methodology identical to that approved by the NRC for operating BWRs, as described in NEDE-32906P. The report TRACG Application for ESBWR, NEDC-33083P (Item 12, Enclosure 1), completes the package. GE is seeking a single NRC SER on the package, for the application of TRACG to the ESBWR SSAR to be used for Design Certification.

If you have any questions about the information provided here, please contact Atam Rao at (408) 925-1885, or myself.

Sincerely,

  
C.J. Deacon

Enclosures

- (1) List of Reports in Support of ESBWR Pre-application Review

cc: A. Cabbage USNRC (with enclosures and CD)  
J. Lyons USNRC (w/o enclosures)  
G.B. Stramback GE (with enclosures and CD)

## Enclosure 1


### List of Reports in Support of ESBWR Pre-application Review

1. ESBWR Design Description, NEDC-33084  
Reference document that defines the ESBWR reference design – **not for review**.
2. ESBWR Test and Analysis Program Description (TAPD), NEDC 33079, Revision 0  
A road map for the technology program that includes PIRT, adequacy of test program and TRACG qualification plan. A similar document was **reviewed for SBWR** and the **testing plan was found acceptable**.
3. TRACG Model Description. NEDE-32176P, Rev.2  
This report has been **reviewed and approved** for operating plants.
4. TRACG Qualification, NEDE-32177P, Revision 2.  
This report has been **reviewed and approved** for operating plants
5. TRACG Qualification for SBWR, NEDC-32725P, Revision 1, Vol.1 and 2  
This report contains TRACG comparisons to test data covering extensive passive system testing that was described and found acceptable for SBWR.
6. TRACG Qualification for ESBWR, NEDC-33080, Revision 0  
This report covers ESBWR specific testing and extends the passive system qualification of TRACG.
7. SBWR Testing Summary Report, NEDC-32606P, Revision 0  
This report covers a summary of all BWR passive system testing and interrelations between tests, that are discussed in detail in item 8 below.
8. Test Reports for Passive Safety Systems  
This covers all previously submitted reports on the passive systems testing for SBWR.
9. ESBWR Test Report, NEDC-33081, Revision 0  
This report covers integral PCCS systems tests done for the ESBWR configuration. **New testing** done at PSI.
10. ESBWR Scaling Report, NEDC-33082P, Revision 0  
Addresses the scaling basis for passive safety systems test programs. Based on previously **NRC reviewed SBWR** scaling report

11. TRACG Application for Anticipated Operational Occurrences Transient Analyses, NEDE-32906P  
This TRACG application methodology for BWR AOO transients was **reviewed and approved** by the NRC for operating plants.
12. TRACG Application for ESBWR, NEDC-33083P, Revision 0  
This covers the TRACG application approach for AOO transient, LOCA and containment analysis. Transient analysis based on approved operating plant application; others based on bounding approach.

# TRACG Qualification for ESBWR

J.R. Fitch  
T. Bandurski  
Y.K. Cheung  
J. Dreier  
R.E. Gamble  
J.M. Healzer  
M. Huggenberger  
L. Klebanov

Approved:   
C.J.W. Deacon, Manager  
Advanced Reactor Projects

**IMPORTANT NOTICE REGARDING  
CONTENTS OF THIS REPORT**

**PLEASE READ CAREFULLY**

Neither the General Electric Company nor any of the contributors to this document:

- a. Makes any warranty or representation, express or implied, with respect to the accuracy, completeness, or usefulness of the information contained in this document, or that the use of any information, apparatus, method, or process disclosed in this document may not infringe privately owned rights;
- or
- b. Assumes any liabilities, including but not limited to nuclear liability, with respect to the use of, or for damages resulting from the use of any information, apparatus, method, or process disclosed in this document.

This work was performed partially as part of a contract between various utilities and GE for “ESBWR Development”.

## Table of Contents

	<b>Page</b>
<b>List of Tables</b>	<b>iv</b>
<b>List of Figures</b>	<b>v</b>
<b>Acronyms</b>	<b>vii</b>
<b>1. INTRODUCTION</b>	<b>1-1</b>
<b>1.1 References</b>	<b>1-4</b>
<b>2. PANDA TRANSIENT TESTS P1-P8</b>	<b>2-1</b>
<b>2.1 Introduction</b>	<b>2-1</b>
<b>2.2 Test Facility and Test Matrix</b>	<b>2-1</b>
<b>2.3 Applicability of Data to ESBWR</b>	<b>2-4</b>
2.3.1 Overview of Data Applicability	2-4
2.3.2 PIRT Phenomena and Coverage	2-7
2.3.3 Conclusions on Data Applicability	2-11
<b>2.4 PANDA TRACG Input Model Description</b>	<b>2-11</b>
2.4.1 RPV, DW, WW, GDSCS and PCC Pools	2-11
2.4.2 IC and PCCS Condensers and Piping	2-12
2.4.3 Main Vents, Vacuum Breakers and GDSCS Lines	2-13
2.4.4 System Line Flow Resistance	2-13
2.4.5 Component Heat Losses and Heat Capacity	2-13
2.4.6 Decay Heat	2-14
2.4.7 Initialization and Control	2-14
<b>2.5 Results of Post-Test Calculations</b>	<b>2-15</b>
2.5.1 Test P1/8	2-17
2.5.1.1 DW and WW Pressures	2-17
2.5.1.2 PCCS Performance	2-18
2.5.1.3 DW and WW Temperatures	2-19
2.5.2 Test P2	2-19
2.5.2.1 DW and WW Pressures	2-20
2.5.2.2 PCCS Performance	2-20
2.5.2.3 DW and WW Temperatures	2-21
2.5.3 Test P3	2-21
2.5.3.1 DW and WW Pressures	2-21
2.5.3.2 PCCS Performance	2-22
2.5.3.3 DW and WW Temperatures	2-23

## Table of Contents (continued)

	<b>Page</b>
2.5.4 Test P4	2-23
2.5.4.1 DW and WW Pressures	2-23
2.5.4.2 PCCS Performance	2-24
2.5.4.3 DW and WW Temperatures	2-25
2.5.5 Test P5	2-25
2.5.5.1 DW and WW Pressures	2-25
2.5.5.2 PCCS Performance	2-26
2.5.5.3 DW and WW Temperatures	2-26
2.5.6 Test P6	2-26
2.5.6.1 DW and WW Pressures	2-27
2.5.6.2 ICS and PCCS Performance	2-27
2.5.6.3 DW and WW Temperatures	2-27
2.5.7 Test P7	2-28
2.5.7.1 DW and WW Pressures	2-28
2.5.7.2 PCCS Performance	2-29
2.5.7.3 DW and WW Temperatures	2-29
2.5.8 Accuracy of TRACG Predictions	2-30
<b>2.6 Summary and Conclusions</b>	<b>2-30</b>
2.6.1 Purpose and Scope of Post-Test Evaluation	2-30
2.6.2 Evaluation of TRACG Qualification Needs	2-31
2.6.2.1 PCC Flow/Pressure Drop (PC1)	2-31
2.6.2.2 Condensation/Condensation-Degradation on Primary Side (PC2)	2-31
2.6.2.3 Secondary-Side Heat Transfer (PC3)	2-32
2.6.2.4 Parallel PCC Tube Effects (PC4)	2-32
2.6.2.5 Parallel PCC Unit Effects (PC5 and XC5)	2-33
2.6.2.6 PCCS Startup (PC8)	2-33
2.6.2.7 DW Multi-Dimensional Effects (DW3)	2-33
2.6.2.8 WW Free Surface Condensation/Evaporation (WW4)	2-34
2.6.2.9 Pool Mixing and Stratification (WW6)	2-35
2.6.2.10 WW Multi-Dimensional Effects (WW7)	2-36
2.6.2.11 Leakage Between DW and WW (DWB1)	2-36
2.6.2.12 System Interaction Effects (IC/DPV/GDCS/PCCS)	2-36
2.6.3 Summary of Conclusions	2-37
<b>2.7 References</b>	<b>2-38</b>
Attachment A to Section 2	2-70



**Table of Contents (continued)**

	<b>Page</b>
<b>3. SIRIUS TWO-PHASE FLOW INSTABILITY TESTS</b>	<b>3-1</b>
<b>3.1 Introduction</b>	<b>3-1</b>
<b>3.2 Test Facility and Test Matrix</b>	<b>3-1</b>
<b>3.3 Applicability of Data to ESBWR</b>	<b>3-2</b>
3.3.1 Overview of Data Applicability	3-2
3.3.2 PIRT Phenomena and Coverage	3-2
<b>3.4 SIRIUS TRACG Input Model and Test Simulation</b>	<b>3-3</b>
<b>3.5 Results of Post-Test Calculations</b>	<b>3-3</b>
3.5.1 Steady-State and Transient Behavior at 2.0 MPa	3-3
3.5.2 Stability Map at 2.0 MPa	3-4
3.5.3 Transient Behavior at 7.2 MPa	3-4
3.5.4 Stability Map at 7.2 MPa	3-5
3.5.5 Comparison of Nominal Operating Conditions to Stability Map	3-5
<b>3.6 Accuracy of TRACG Calculations</b>	<b>3-5</b>
<b>3.7 Summary and Conclusions</b>	<b>3-5</b>
<b>3.8 References</b>	<b>3-7</b>

## List of Tables

		<b>Page</b>
Table 2-1	PANDA/TRACG VSSL01 Component Breakdown	2-39
Table 2-2	Comparison of PANDA and ESBWR Component Nodalizations	2-39
Table 2-3	Initial Conditions for PANDA Test P1/8 (Test Report/TRACG Input)	2-40
Table 2-4	Initial Conditions for PANDA Test P2 (Test Report/TRACG Input)	2-40
Table 2-5	Initial Conditions for PANDA Test P3 (Test Report/TRACG Input)	2-40
Table 2-6	Initial Conditions for PANDA Test P4 (Test Report/TRACG Input)	2-40
Table 2-7	Initial Conditions for PANDA Test P5 (Test Report/TRACG Input)	2-41
Table 2-8	Initial Conditions for PANDA Test P6 (Test Report/TRACG Input)	2-41
Table 2-9	Initial Conditions for PANDA Test P7 (Test Report/TRACG Input)	2-41
Table 2-10	PCC Instrumentation for PANDA Post-Test Evaluation	2-42
Table 2-11	DW Instrumentation for PANDA Post-Test Evaluation	2-43
Table 2-12	WW Instrumentation for PANDA Post-Test Evaluation	2-44
Table 2-13	Oxygen Probe Instrumentation for PANDA Post-Test Evaluation	2-45
Table 2-14	IC Instrumentation for PANDA Post-Test Evaluation	2-45
Table 2-15	RPV and GDCS Level Instrumentation for PANDA Post-Test Evaluation	2-45
Table 2-16	PANDA Measurement Uncertainties	2-46
Table 2-17	Assessment of TRACG Accuracy for PANDA Transient (P-Series) Tests	2-46
Table 3-1	Assessment of TRACG Accuracy for CRIEPI/SIRIUS Flow Instability Tests	3-8

## List of Figures

		<b>Page</b>
Figure 2-1.	PANDA Test Facility Schematic	2-47
Figure 2-2.	TRACG Model for ESBWR Long-Term Containment Cooling Transient	2-48
Figure 2-3.	TRACG VSSL Component for PANDA RPV, DW, WW (SC), GDCS and Condenser Pools	2-49
Figure 2-4.	TRACG Model for RPV RISER (TEE09), RPV Heater (CHAN08), and Main Steam Lines (VLVE19 AND VLVE20)	2-50
Figure 2-5.	TRACG Models for DW, WW (SC) and SP Connecting Pipes	2-51
Figure 2-6.	TRACG Model for PCCS for Tests with Air as the Only Noncondensable	2-52
Figure 2-7.	TRACG MODEL for IC	2-53
Figure 2-8.	TRACG MODEL for PCC Inlet Lines	2-54
Figure 2-9.	TRACG MODEL for PCC Drain Lines	2-55
Figure 2-10.	TRACG MODEL for PCC Vent Lines	2-56
Figure 2-11.	TRACG MODEL for IC Inlet Line	2-57
Figure 2-12.	TRACG MODEL for IC Drain Line	2-58
Figure 2-13.	TRACG MODEL for IC Vent Line	2-59
Figure 2-14.	TRACG MODEL for PCC Drain to IC Drain Connecting Lines	2-60
Figure 2-15.	TRACG PCC MODEL for Test P7 With Helium	2-61
Figure 2-16.	TRACG Models for Main Vent Lines	2-62
Figure 2-17.	TRACG Model for VB1	2-63
Figure 2-18.	TRACG Model for VB2	2-64
Figure 2-19.	TRACG Model for GDCS Drain Line	2-65
Figure 2-20.	TRACG Model for GDCS to WW Connection Lines	2-66
Figure 2-21.	GDCS, DW, WW (SC) and SP Instrumentation Superimposed on TRACG Nodalization	2-67
Figure 2-22.	PCC1 Instrumentation Superimposed on TRACG Nodalization	2-68
Figure 2-23.	IC Instrumentation Superimposed on TRACG Nodalization	2-69
Figure 3-1.	Schematic Diagram of the Sirius Thermal Hydraulic Test Facility	3-9
Figure 3-2.	TRACG Model of Sirius Test Facility	3-9
Figure 3-3.	Comparison of Measured and Calculated Steady-State Inlet Velocities as A Function of Inlet Subcooling at 2.0 MPA and 190 KW/ M2	3-10
Figure 3-4.	Observed Effect of Inlet Subcooling on Circulation Flow at 2.0 MPA and 190 KW/ M2	3-10
Figure 3-5.	TRACG Calculation of the Effect of Inlet Subcooling on Circulation Flow at 2 MPA and 190 KW/M2	3-11
Figure 3-6.	Comparison of Measured and Calculated Channel Inlet Velocity at 2 MPA and 190 KW/M2 with Inlet Subcooling of 22.3K	3-11
Figure 3-7.	Comparison of Measured and Calculated Average Void Fractions In Regions 7 and 8 AT 2 MPA And 190 KW/M2 With Inlet Subcooling of 22.3 K	3-12
Figure 3-8.	Comparison of Measured and Calculated Channel Inlet Velocity At 2 MPA and 457 KW/M2 with Inlet Subcooling Of 48.6 K	3-12

### List of Figures (continued)

		<b>Page</b>
Figure 3-9.	Comparison of Measured and Calculated Average Void Fractions In Regions 7 and 8 at 2 MPA and 457 KW/M2 with Inlet Subcooling of 48.6 K	3-13
Figure 3-10.	Comparison of Calculated and Observed Stability Maps At 2.0 MPA	3-13
Figure 3-11.	Observed Effect of Inlet Subcooling on Circulation Flow at– 7.2 MPA and 760 KW/ M2	3-14
Figure 3-12.	TRACG Calculation of The Effect of Inlet Subcooling on Circulation Flow at 7.2 MPA and 760 KW/M2	3-14
Figure 3-13.	Comparison of Measured and Calculated Channel Inlet Velocity at 7.2 MPA AND 760 KW/M2 with Inlet Subcooling of 90.4	3-15
Figure 3-14.	Comparison of Measured and Calculated Average Void Fractions in Regions 7 and 8 at 7.2 MPA and 760 KW/M2 with Inlet Subcooling of 90.4 K	3-15
Figure 3-15.	Comparison of Calculated and Observed Stability Maps at 7.2 MPA	3-16

### Acronyms

BWR	Boiling Water Reactor
CRIEPI	Central Research Institute for Electric Power Industry
DPV	Depressurization Valve
DW	Drywell
ECCS	Emergency Core Cooling System
EQL	Equalization Line
ESBWR	European Simplified Boiling Water Reactor
GDCS	Gravity-Driven Cooling System
GE	General Electric Company
IC	Isolation Condenser
ICS	Isolation Condenser System
LOCA	Loss-of-Coolant Accident
MSL	Main Steam Line
MSLB	Main Steam Line Break
PANDA	<u>P</u> assive <u>N</u> achwarmeabfuhr-und <u>D</u> rueckabbau-Testanlage
PANTHERS	<u>P</u> erformance <u>A</u> nalysis and <u>T</u> esting of <u>H</u> eat <u>R</u> emoval <u>S</u> ystems
PCC	Passive Containment Condenser
PCCS	Passive Containment Cooling System
PIRT	Phenomena Identification and Ranking Table
PSI	Paul Scherrer Institute
RPV	Reactor Pressure Vessel
SBWR	Simplified Boiling Water Reactor
SC	Pressure Suppression Chamber
SIRIUS	<u>S</u> imulated <u>R</u> eactivity Feedback <u>I</u> ncorporated with Thermal-Hydraulic <u>S</u> tability
SP	Suppression Pool
TAPD	Test and Analysis Program Description
TRACG	Transient Reactor Analysis Code, GE version
VB	Vacuum Breaker
WW	Wetwell

# 1. INTRODUCTION

This report describes qualification studies of the TRACG computer code performed for the European Simplified Boiling Water Reactor (ESBWR). It supplements the material in the generic TRACG qualification report [1-1] and the TRACG qualification report for the SBWR [1-2]. Computer code qualification, as defined at GE Nuclear Energy, incorporates the process of validation of the code against data or alternate engineering calculations. Validation is part of the process of “qualifying” the computer code for design application.

The generic TRACG qualification report [1-1] includes a comprehensive collection of TRACG qualification studies applicable to BWR-related separate effects, component, integral system and reactor tests. These tests cover a wide range of phenomena and configurations representative of BWR conditions for loss-of-coolant accidents (LOCAs), operational transients and density wave oscillation. Most of these test data are also applicable to the ESBWR, as discussed in the ESBWR Test and Analysis Program Description (TAPD) [1-3]. Reference 1-2 supplemented the TRACG generic qualification by documenting an extensive set of validation studies performed as part of the earlier SBWR program. All of the Reference 1-2 studies are considered to be directly applicable to the ESBWR [1-3].

The present report documents two additional validation studies performed specifically in support of the ESBWR. The test data used for these studies are from the P-series containment tests performed at the PANDA test facility in Switzerland and from the elevated-pressure hydrodynamic instability tests performed at the CRIEPI/SIRIUS test facility in Japan. The PANDA P-series tests extended the previous PANDA investigation of SBWR post-LOCA long-term containment cooling to confirm the post-LOCA performance of the higher-power ESBWR with its modified containment configuration. The CRIEPI/SIRIUS tests extended the previous CRIEPI investigation of hydrodynamic instability at low pressure to cover the pressure range from ESBWR startup to full-power operation.

This report is one of several documents that provide the information necessary for the validation of the TRACG computer code and its application for ESBWR design analysis. The relationship of this report to the generic TRACG qualification report [1-1] and the SBWR qualification report [1-2] was addressed above. The other relevant reports are the ESBWR Test and Analysis Program Description [1-3], the ESBWR Test Report [1-4], the ESBWR Scaling Report [1-5], the TRACG Model Description [1-6], and the TRACG Application for ESBWR [1-7]. A unifying element of the ESBWR documentation is reference to a set of “PIRT” phenomena that have been judged to be of significance for the calculation of ESBWR safety parameters. The PIRT acronym derives from the Phenomena Identification and Ranking Tables that are used to identify and prioritize the phenomena in relation to the safety parameters.

TRACG is being qualified for ESBWR licensing analyses of operational transients, LOCA-ECCS and LOCA-containment. A detailed description of the application methodology is provided in Reference 1-7. There are differences in the application approach for the three types of events. Operational transients are being addressed within the framework of the Code Scaling, Applicability and Uncertainty (CSAU) methodology [1-8]. For LOCA-ECCS, the CSAU process will be followed to identify the uncertainties in the TRACG models, correlations and parameters

that govern the prediction of the minimum water level. It will then be demonstrated that these uncertainties can be combined in such a way as to produce conservative design evaluations of LOCA-ECCS transients. For LOCA-containment applications, a similar bounding design evaluation methodology will be employed.

The version of the TRACG code utilized for the validation studies described herein is designated as TRACG04. TRACG04 is a configuration-controlled version of TRACG that was used for most of the analyses documented in the SBWR qualification report [1-2]. The qualification studies documented in the generic TRACG qualification report [1-1] and a few of the SBWR qualifications were performed with an earlier code version, designated as TRACG02. Table 1.2-1 of Reference 1-2 lists the version of the code used for each of the qualification studies in References 1-1 and 1-2. The next revision of the TRACG generic qualification report will update the TRACG02 calculations and data comparisons to TRACG04. This revision will be accompanied by revisions of the TRACG Model Description [1-6] and the TRACG User's Manual [1-9].

The ESBWR Test Report [1-4] describes key features of the PANDA P-series tests and the results obtained. The ESBWR Scaling Report [1-5] establishes the fidelity of the PANDA and CRIEPI/SIRIUS test facilities to scale the major ESBWR phenomena and the applicability of the test data to the ESBWR. Changes in nodalization needed to calculate the experiments accurately have been reflected in the TRACG ESBWR plant nodalization.

The results of the qualification assessments lead to evaluations of the model bias and uncertainty in the calculation of important parameters. In this way, code uncertainty is evaluated by a direct comparison of data with code calculations. The contribution due to measurement uncertainty is not explicitly identified in the statistical evaluation of the differences between data and calculations and, as such, is implicitly included in the uncertainty.

Sections 2 and 3 of this report describe, respectively, qualification of TRACG against the PANDA P-series data and the CRIEPI/SIRIUS data. Each qualification section is organized as follows.

- Introduction
  - General description and purpose of tests; tests selected for post-test analysis; purpose of post-test analysis
- Test Facility/Test Matrix
  - Brief description of test facility; summary of test matrix
- Applicability of Data to ESBWR
  - Aspects of ESBWR scenario addressed by the test with reference to PIRT phenomena; range of relevant test parameters vs. ESBWR

- TRACG Model
  - Nodalization of test facility; comparison with ESBWR plant model nodalization
- Test Simulation
  - Method of simulating the test with TRACG; initial and boundary conditions
- Results of Post-Test Calculations
  - Comparison between the test data and TRACG results; discussion of key features of test behavior and TRACG predictions
- Summary and Conclusions
  - Overall assessment of adequacy of TRACG predictions; specific assessment with respect to key PIRT phenomena; implications for TRACG simulation of ESBWR



## 1.1 References

- 1-1. *TRACG Qualification*, NEDE-32177P (Rev. 2), January 2000.
- 1-2. *TRACG Qualification for SBWR*, NEDC-32725P (Rev. 1), August 2002.
- 1-3. *ESBWR Test and Analysis Program Description*, NEDC-33079 (Rev. 0), August 2002.
- 1-4. *ESBWR Test Report*, NEDC-33081P (Rev. 0), August 2002.
- 1-5. *ESBWR Scaling Report*, NEDC-33082P (Rev. 0).
- 1-6. *TRACG Model Description*, NEDE-32176P (Rev. 2), December 1999.
- 1-7. *TRACG Application for ESBWR*, NEDE-33083P (Rev. 0).
- 1-8. *Quantifying Reactor Safety Margins - Application of Code Scaling, Applicability and Uncertainty Evaluation Methodology for a Large-Break Loss-of-Coolant Accident*, NUREG/CR/5249, EGG-2552, 1989.
- 1-9. *TRACG02A User's Manual*, NEDC-32956P (Rev. 0), February 2000.

## 2. PANDA TRANSIENT TESTS P1-P8

### 2.1 Introduction

Reference 2-1 describes a comprehensive qualification of the TRACG computer code [2-2 and 2-3] for analysis of the SBWR. A major element of the TRACG SBWR qualification program was a series of integral systems tests performed in the PANDA test facility at the Paul Scherrer Institute (PSI) in Switzerland. The PANDA facility was designed to model the long-term cooling phase of the SBWR LOCA. It includes the Passive Containment Cooling System (PCCS), the Isolation Condenser System (ICS) and the Gravity Drain Cooling System (GDCCS). The SBWR test matrix (known as the M-series) included, in addition to a design-basis LOCA simulation, a series of tests designed to challenge both the performance of the passive safety systems and the ability of TRACG to predict that performance. The most significant conclusion from the SBWR PANDA qualification activity [2-1] was that TRACG accurately calculates post-LOCA containment pressurization and is well-suited to the calculation of post-LOCA containment transients involving interactions between the passive safety systems.

To support the extension of the TRACG qualification activity to the ESBWR, an ESBWR-specific PANDA test program was performed. The PANDA facility was modified to represent the ESBWR and a test matrix, designated as the “P-series”, was defined. The P-series consisted of eight transient tests representing design-basis and beyond design-basis post-LOCA conditions [2-4]. The purpose of this section is to present the results of TRACG post-test calculations for the P-series tests as an extension to the qualification reported in Reference 2-1. The post-test analyses of the transient tests were performed by an ESBWR PANDA analysis team, with participation from PSI in Switzerland, where the tests were conducted, and the General Electric Company (GE) in the United States. The calculations were performed with the TRACG04 version of the code.

The remainder of this section is organized as follows. Section 2.2 presents a brief description of the PANDA test facility and the P-series test matrix. Section 2.3 discusses the applicability of the PANDA transient data to the ESBWR and includes a rationale for each of the P-series tests. Section 2.4 provides a description of the PANDA TRACG input model used for the post-test analyses. For each test, there is a summary table of the measured thermodynamic conditions at the start of the test which were used for the initialization of the various components in the TRACG model. Section 2.5 presents the results of the post-test calculations on a test-by-test basis and includes a quantitative evaluation of the accuracy of the TRACG predictions. Section 2.6 discusses the results of the study with reference to key ESBWR phenomena and presents a final set of conclusions.

### 2.2 Test Facility and Test Matrix

The PANDA test facility was originally designed to model the long-term cooling phase of the loss-of-coolant accident (LOCA) for the SBWR. In its original configuration, it was a 1/25 volume-scaled, full-height simulation of the SBWR primary system and containment and included the major components necessary to simulate the SBWR system response during the long-term phase of the LOCA. These components include the containment drywell (DW), the

wetwell (WW) or suppression chamber, the reactor pressure vessel (RPV) including the core, and those safety systems that would operate during the long-term phase of the LOCA. Important passive safety systems modeled in PANDA include the Passive Containment Cooling System (PCCS), Isolation Condenser System (ICS) and the Gravity-Driven Cooling System (GDCS). Fluids are either prototypical (water and steam) or close to prototypical (air and helium).

The RPV is represented by a single vessel in PANDA whereas the DW and WW are represented by pairs of vessels, connected by large pipes. This double-vessel arrangement permits simulation of spatial distribution effects within the containment volumes. The water in the RPV is heated by a bank of controlled electrical heaters that can be programmed to match the decay heat curve. Main steam lines (MSLs) convey boiloff steam from the RPV to the two DW vessels. Three scaled passive containment condensers (PCCs) and one scaled isolation condenser (IC) are located in individual water pools on the roof above the DW vessels. The PCC and IC inlet lines are connected to the DW and RPV vessels, respectively. Drain lines from the lower headers of the PCCs and IC return condensate to the RPV. Vent lines from the lower headers of the PCCs and the upper and lower headers of the IC connect at prototypical submergences in the suppression pools (SPs). Vacuum breakers (VBs) were installed in the lines connecting the DW and WW gas spaces. PANDA has the capability to valve out one of the MSLs, the IC and individual PCCs.

A schematic of the PANDA test facility as configured for the ESBWR is shown in Figure 2-1. The PANDA power/volume scaling for the ESBWR is nominally 1:45. Heights and submergences are scaled at approximately 1:1. The PANDA PCCS uses three independent loops and condenser units to represent the four-loop ESBWR PCCS. The PANDA ICS uses one loop and condenser to represent the four-loop ESBWR ICS. The GDCS pool is represented by a separate vessel in PANDA. A major alteration of PANDA for the ESBWR was to connect the GDCS gas space to the WW gas space. This ESBWR design modification provides a larger repository for the noncondensable gas that is swept from the DW to the WW during the blowdown and thereby reduces the containment pressure. The piping interconnecting the PANDA vessels is scaled (primarily with the use of orifice plates) to produce the same pressure loss as the corresponding ESBWR piping at the scaled ESBWR flow rate.

A brief description of the accident scenario for an ESBWR MSLB is useful as background for the discussion of the P-series test matrix. During the initial depressurization phase, steam is discharged through the MSLB from the RPV to the DW, where the steam is mixed with nitrogen that fills the DW under normal operating conditions. The major portion of the steam is vented through the main vents and condensed in the SP, raising the SP temperature. The remainder flows to the PCCS and is mostly condensed by the PCC units with heat rejection to the condenser pools. The vented nitrogen from both flow paths is accumulated in the WW gas space. At about 15 minutes from accident initiation, discharge of GDCS water to the RPV is initiated. Injection of subcooled GDCS water in conjunction with PCCS heat removal causes the DW pressure to drop below the WW pressure resulting in a VB opening and return of steam and non-condensables to equalize DW and WW pressures. At about one hour from accident initiation decay power overcomes the effect of the subcooled GDCS water, steaming from the RPV to the DW resumes and the decay heat load shifts to the PCCS. This marks the start of the long-term

cooling phase and represents the starting point for most of the PANDA simulations of ESBWR post-LOCA behavior.

The long-term cooling phase of the LOCA is defined as starting at one hour from the occurrence of the break. Conditions at this time in the LOCA transient were derived from ESBWR TRACG calculations. The calculations show that the one-hour thermodynamic conditions throughout the system are relatively stable. The effect of subcooling of RPV water by GDSCS injection is just on the verge of being overcome by the decay power. The pressure difference between the RPV and DW is just sufficient to maintain flow of the boiloff steam through the break and the open depressurization valves. To remove the energy added to the DW, the PCCS must first purge residual noncondensable gases from the DW to the WW and, accordingly, the pressure difference between the DW and WW is just sufficient to clear the PCC vents.

One of the compromises made in the original design of the PANDA test facility was to not scale the volume of water available to replace boiloff in the SBWR and, by extension, the ESBWR PCCS. In the ESBWR, this volume, which extends outside the individual PCC pools, is sufficient to maintain coverage of no less than 50% of the condenser tube length for 72 hours. In PANDA, only the water in the four individual pools (three PCC pools and one IC pool) is available to replace boiloff. Capability was originally provided to either interconnect or isolate the individual pools and to provide replacement water through fittings in the pool bottoms. It was subsequently decided that the ability to directly assess individual PCC and IC heat transfer through the boildown of the individual pools outweighed the advantage of allowing refill from the pools for condenser units (typically, the IC) that were not in service for a given test. With the exception of Test P1/8, the duration of the P-series tests was short enough to preclude uncovering of the condenser tubes by pool boildown.

The P-series test matrix is described in detail in Reference 2-4. Test P1 was a base-case simulation of the ESBWR LOCA long-term cooling phase following a MSLB. Subsequent tests incorporated variations of key parameters and addressed specific thermal-hydraulic phenomena which are considered to be of potential importance for calculation of long-term post-LOCA behavior in the ESBWR. Test P2 was configured to start at an earlier time in the transient and provided data during the transition from the GDSCS injection phase to the long-term cooling phase. Test P3 demonstrated PCCS start-up capability with initially non-condensable-filled DW vessels and PCC units, representing the upper limit of initial DW noncondensable inventory. In addition, Test P3 examined the influence of asymmetric distributions of steam and air in the DW on the startup and long-term performance of the PCCS by releasing all of the RPV steam to DW2. To further challenge the system, the PCC unit on DW1 was valved out of service. Test P4 included the delayed release of non-condensable gas into the DW to simulate the effect of noncondensable hideout in regions of the ESBWR DW that are not directly exposed to mixing by the steam jets emanating from the RPV. Test P5 was similar to Test P4 but further challenged the system by valving one of the PCC units out of service. Test P6 considered system interaction effects associated with parallel operation of the PCCS and ICS and the effect of a postulated direct bypass of steam from the DW to the WW air space. Test P6 was started with the Isolation Condenser (IC) in operation in parallel with the PCCs. Later in the test, a DW-to-WW leakage path was opened to simulate a possible steam bypass. At a still later time, the IC was valved out,

shifting the portion of the decay heat load that was being carried by the ICS to the PCCS. In test P7, helium was injected in DW1 a few hours after test initiation, providing data on the performance of the PCCS in the presence of noncondensables lighter than steam. Test P8, performed as an extension of Test P1, simulated the system behavior with PCC pool water levels below the bottom of the condenser upper headers.

## **2.3 Applicability of Data to ESBWR**

This section describes how the PANDA P-series tests provided relevant data for validation of computer models used to analyze the post-LOCA containment performance of the ESBWR. The PANDA P-series test objectives and the general applicability of the data to the ESBWR are discussed in Section 2.3.1. Descriptions of the PIRT phenomena and associated parameters covered by the PANDA P-series tests are given in Section 2.3.2.

### **2.3.1 Overview of Data Applicability**

The objective of the PANDA P-series Test Program was to provide a database to confirm the capability of TRACG to calculate ESBWR containment system performance (including potential systems interaction effects) and to demonstrate startup and long-term operation of the PCCS. As in the case of the earlier SBWR M-series tests, the testing philosophy was based on identification of a “Base-Case” test around which perturbations were made to assess the effects of specific systems, systems interactions, and phenomena of interest.

#### **Test P1 (Base Case) and Test P8 (Pool Boildown)**

The base case (Test P1) was a simulation of the long-term cooling phase following a LOCA caused by a guillotine rupture of one of the main steam lines. This LOCA scenario leads to the highest long-term containment pressure in the ESBWR. A key identifying feature of Test P1 was equal steam flow from the RPV to each of the two PANDA DW vessels. Test P8 was performed as an extension of Test P1 and examined PCCS performance with boildown of the condenser pools below the bottom of the condenser upper headers. The combination of Tests P1 and P8 is designated as Test P1/8.

#### **Test P2 (Early Start)**

The PANDA facility was originally designed to simulate the long-term cooling phase of the post-LOCA transient. All of the tests in the PANDA matrix, with the exception of Test P2, examine PCCS performance under various conditions following the initiation of the long-term cooling phase. As a result of detailed evaluation of the various elements of the overall ESBWR test program, it was decided that one of the PANDA tests should simulate PCCS behavior and system interactions during the transitional period from the end of the blowdown to the initiation of long-term cooling. With this objective in mind, conditions for Test P2 were developed to examine PCCS performance during the portion of the post-LOCA transient extending from the GDSC injection phase into the long-term cooling phase.

Based on analysis and understanding of ESBWR post-LOCA performance, the following sequence of events is expected during the period simulated by PANDA Test P2. As GDSC

injection proceeds, steam flow from the RPV to the DW is reduced, the DW pressure falls and the flow to the PCCS is reduced. The decreasing DW pressure opens a VB and allows the return of noncondensable gas to the DW from the WW. As the rate of GDCS injection decreases and the RPV inventory heats up to saturation, the DW re-pressurizes and flow to the PCCS resumes. This marks the initiation of the long-term cooling phase at about one hour from the start of the LOCA. By simulating the portion of the post-LOCA transient described above, Test P2 addressed systems interactions between the PCCS, GDCS, and the VBs.

It was recognized, from the outset that Test P2 would involve some scaling compromises relative to the rest of the PANDA test matrix. These compromises result from (1) the upper limit of the PANDA heater output (1.4 MW), (2) the fact that the GDCS pool is not fully scaled to the ESBWR, and (3) a design limitation of the test facility which does not permit liquid flow from the RPV to the DW through the steam lines. The initial conditions and heater power were selected to achieve the objectives of Test P2 within the constraints imposed by the test facility.

### **Test P3 (DW and PCCS Initially Filled with Noncondensable)**

The main purpose of Test P3 was to address the issue of PCCS startup and operation from a condition representing the upper limit of initial DW noncondensable inventory. Every known analysis of an RPV blowdown into a BWR containment indicates that, within a matter of seconds, essentially all of the initial inventory of the DW inerting gas is forced into the WW, leaving the DW with a nearly pure-steam environment. Thus, when the ESBWR PCCS is called upon to assume the decay heat load, it is expected that it will face a minimal challenge from residual noncondensable gas in the inlet mixture. It is certainly possible for gas to “hide out” in various dead-end regions of the DW and subsequently find its way to the PCCS inlet lines (see description of Tests P4 and P5), but this is a long-term process which would not be expected to interfere with initial PCCS operation at high decay heat load. [

Redacted

]

The above considerations notwithstanding, it is of interest to consider what would happen if the PCCS was confronted with the ultimate challenge of peak (one-hour) decay heat load and a DW essentially filled with noncondensable gas. The initial distribution of air for Test P3 was determined by postulating that the initial blowdown raised the temperature of the SP to 354 K and that the DW was filled with dry air at 301 K. The heatup of the WW pool, which increases the steam pressure in the WW air space, means that the DW air inventory is actually higher than it would be during normal operation and explains why the initial DW pressure (129 kPa) is above atmospheric pressure. As a final step toward making this a truly bounding case, the RPV power was held constant at 0.85 MW, rather than allowing it to follow the decay heat curve. This was partly done to compensate for the fact that the DW walls are cold at the start of the test and some power will be required to bring them up to temperature.

A secondary purpose of Test P3 was to simulate the effect of steam flowing preferentially to one side of the DW in the ESBWR by forcing all of the RPV steam to flow to DW2 and by valving out the PCC unit (PCC1) attached to DW1. A major design objective of the PCCS is that the system should be “robust” in the sense of being able to adjust to a wide range of inlet

conditions, including those associated with nonuniform distributions of steam and noncondensable gas in the DW. Directing all the RPV steam to DW2 and shutting off the PCC unit on DW1 creates the maximum degree of asymmetry in the PANDA DW. Shutting off one PCC unit and running at constant power puts the PCCS in an overload condition. The combination of asymmetric steam flow, limiting initial DW noncondensable inventory and PCCS overload addresses the objective of a robust PCCS.

#### **Tests P4 and P5 (Delayed Release of DW Noncondensable)**

Tests P4 and P5 further address the issue of PCCS robustness by considering the effect of a delayed release of noncondensable gas from DW “hideout” regions where it may have been trapped during the initial blowdown and subsequent PCCS purging. The initial conditions for both Tests P4 and P5 are nominally the same as for the base case Test P1. Starting at four hours from test initiation, air was injected to DW1 for 30 min. Test P5 differed from Test P4 by having one of the two PCCs (PCC2) on DW2 shut off. These tests demonstrated PCCS performance when the system has been operating in balance with the RPV heat load and is abruptly forced to deal with the degrading effect of noncondensable in the inlet flow. Test P5 increases the challenge by shutting off one of the PCC units. Finally, Test P4 serves as a repeat of the base case Test P1 for the four hours that precede the air injection.

#### **Test P6 (ICS/PCCS Interaction and VB Leakage)**

Test P6 considered system interaction effects associated with parallel operation of the ICS and PCCS and the effect of a direct bypass of steam from the DW to the WW air space. Both of these effects are directly applicable to design-basis evaluation of PCCS performance following a postulated LOCA in the ESBWR. In the ESBWR, the ICS would automatically come into operation on a low RPV water level signal and would immediately start condensing RPV steam, operating in parallel with the PCCS. The only uncertainty is whether the IC vents would be opened because this operation must be performed by the operator. Not opening the vents could lead to ICS shutdown from accumulation of noncondensable. To cover this possibility in Test P6, the IC was valved out of service after seven hours of operation. This guaranteed that the test would address the situation in which, after an initial period of IC operation, the decay heat load must be shifted from the ICS to the PCCS.

Bypass leakage from the DW to the WW air space is a design consideration in the ESBWR. During portions of the long-term cooling transient, operation of the PCCS requires a sufficient pressure difference between the DW and WW to keep the PCCS vents open. If a leakage path between the DW and WW existed, this pressure difference would sustain a parallel bypass leakage flow. The ESBWR design, particularly with regard to the VBs, has gone to great lengths to ensure that no DW-to-WW leakage path is possible. For design basis accident evaluations, however, a leakage path with an effective  $A/\sqrt{K}$  of  $1 \text{ cm}^2$  is considered. Test P6 was performed with a scaled leakage path equivalent to approximately  $20 \text{ cm}^2$  in the ESBWR. The inclusion of a leakage path with 20 times the effective area of the ESBWR design leakage provided confirmation that bypass leakage, in the unlikely event that it exists, will, at most, result in a gradual increase in system pressure that would allow adequate time for other remedial actions to be taken.

**Test P7 (Lighter-Than-Steam Noncondensable)**

Test P7 investigated PCCS performance under a challenging set of circumstances that might be associated with a severe accident scenario. The initial conditions were as predicted for the ESBWR at one hour from the instant of the LOCA. An asymmetric overload condition was set up by releasing all of the RPV steam to DW2 and by valving out the PCC unit (PCC1) on DW1. Four hours from test initiation, helium was injected to DW1 for a period of two hours. This presented the PCCS with the dual challenge of dealing with the delayed release of a lighter-than-steam noncondensable gas with one unit removed from service.

**2.3.2 PIRT Phenomena and Coverage**

[

Redacted

]



[

Redacted

]

[

Redacted

]

[

Redacted

]

**2.3.3 Conclusions on Data Applicability**

[

Redacted

]

**2.4 PANDA TRACG Input Model Description**

[

Redacted

]

**2.4.1 RPV, DW, WW, GDCS and PCC Pools**

[

Redacted

]

[

Redacted

]

**2.4.2 IC and PCCS Condensers and Piping**

[

Redacted

]

[

Redacted

]

**2.4.3 Main Vents, Vacuum Breakers and GDCS Lines**

[

Redacted

]

**2.4.4 System Line Flow Resistance**

[

Redacted

]

**2.4.5 Component Heat Losses and Heat Capacity**

[

Redacted

]

[

Redacted

]

#### **2.4.6 Decay Heat**

[

Redacted

]

#### **2.4.7 Initialization and Control**

[

Redacted

]

[

Redacted

]

## **2.5 Results of Post-Test Calculations**

[

Redacted

]



[

Redacted

]

[

Redacted

]

**2.5.1 Test P1/8**

[

Redacted

]

**2.5.1.1 DW and WW Pressures**

[

Redacted

]

[

Redacted

]

**2.5.1.2 PCCS Performance**

[

Redacted

]

[

Redacted

]

### **2.5.1.3 DW and WW Temperatures**

[

Redacted

]

### **2.5.2 Test P2**

[

Redacted

]

[ Redacted ]

**2.5.2.1 DW and WW Pressures**

[ Redacted ]

**2.5.2.2 PCCS Performance**

[ Redacted ]

[ ]

**2.5.2.3 DW and WW Temperatures**

[ ]

Redacted

**2.5.3 Test P3**

[ ]

Redacted

**2.5.3.1 DW and WW Pressures**

[ ]

Redacted

]

[

Redacted

]

**2.5.3.2 PCCS Performance**

[

Redacted

]





[

Redacted

]

#### **2.5.4.2 PCCS Performance**

[

Redacted

]

**2.5.4.3 DW and WW Temperatures**

[

Redacted

]

**2.5.5 Test P5**

[

Redacted

]

**2.5.5.1 DW and WW Pressures**

[

Redacted

]

**2.5.5.2 PCCS Performance**

[

Redacted

]

**2.5.5.3 DW and WW Temperatures**

[

Redacted

]

**2.5.6 Test P6**

[

Redacted

]

**2.5.6.1 DW and WW Pressures**

[

Redacted

]

**2.5.6.2 ICS and PCCS Performance**

[

Redacted

]

**2.5.6.3 DW and WW Temperatures**

[

Redacted

]

[

Redacted

]

**2.5.7 Test P7**

[

Redacted

]

**2.5.7.1 DW and WW Pressures**

[

Redacted

]

[

Redacted

]

### **2.5.7.2 PCCS Performance**

[

Redacted

]

### **2.5.7.3 DW and WW Temperatures**

[

Redacted

]

[ Redacted ]

**2.5.8 Accuracy of TRACG Predictions**

[ Redacted ]

**2.6 Summary and Conclusions**

**2.6.1 Purpose and Scope of Post-Test Evaluation**

[ Redacted ]

[ Redacted ]

**2.6.2 Evaluation of TRACG Qualification Needs**

[ Redacted ]

**2.6.2.1 PCC Flow/Pressure Drop (PC1)**

[ Redacted ]

**2.6.2.2 Condensation/Condensation-Degradation on Primary Side (PC2)**

[ Redacted ]



[

Redacted

]

**2.6.2.3 Secondary-Side Heat Transfer (PC3)**

[

Redacted

]

**2.6.2.4 Parallel PCC Tube Effects (PC4)**

[

Redacted

]

[

Redacted

]

**2.6.2.5 Parallel PCC Unit Effects (PC5 and XC5)**

[

Redacted

]

**2.6.2.6 PCCS Startup (PC8)**

[

Redacted

]

**2.6.2.7 DW Multi-Dimensional Effects (DW3)**

[

Redacted

]

[

Redacted

]

**2.6.2.8 WW Free Surface Condensation/Evaporation (WW4)**

[

Redacted

]

[

Redacted

]

**2.6.2.9 Pool Mixing and Stratification (WW6)**

[

Redacted

]

[  
Redacted  
]

**2.6.2.10 WW Multi-Dimensional Effects (WW7)**

[  
Redacted  
]

**2.6.2.11 Leakage Between DW and WW (DWB1)**

[  
Redacted  
]

**2.6.2.12 System Interaction Effects (IC/DPV/GDCS/PCCS)**

[  
Redacted  
]

**2.6.3 Summary of Conclusions**

[

Redacted

]

## **2.7 References**

- 2-1. *TRACG Qualification for SBWR*, NEDC-32725P (Rev. 1), August 2002.
- 2-2. *TRACG Model Description*, NEDE-32176P (Rev. 2), December 1999.
- 2-3. *TRACG02A User's Manual*, NEDC-32956P (Rev. 0), February 2000.
- 2-4. M. Huggenberger, *PANDA P-Series Test Specification*, ALPHA-703-0, December 1997.
- 2-5. S. Lomperski, *PANDA Facility Characterization, Vessel Heat Loss Measurements*, ALPHA-519-0, November 1997.
- 2-6. *ESBWR Test Report*, NEDC-33081P (Rev. 0), August 2002.
- 2-7. *ESBWR Test and Analysis Program Description*, NEDC-33079 (Rev. 0), August 2002.

**Table 2-1  
PANDA/TRACG VSSL01 Component Breakdown**

[

Redacted

]

**Table 2-2  
Comparison of PANDA and ESBWR Component Nodalizations**

[

Redacted

]



**Table 2-3****Initial Conditions for PANDA Test P1/8 (Test Report/TRACG Input)**

	<b>RPV</b>	<b>Drywell</b>	<b>Wetwell</b>	<b>GDCS</b>	<b>PCC/IC Pools</b>
Total Pressure (bar)	2.61/2.45	2.58/2.45	2.34/2.35	2.32/2.35	0.98/0.98
Air Pressure (bar)(3)	0.0/0.0	0.034/0.045	1.98/2.01	2.19(2)/2.21	N/A
Vapor Temperature (C)	128/128	127/126	71/71	51/51	N/A
Liquid Temperature (C)	128/128	N/A	72/72	N/A	96/96
Collapsed WL (m) (1)	12.6/12.6	0.07/0.0	3.9/3.9	0.09/0.0	4.2/4.2

**Table 2-4****Initial Conditions for PANDA Test P2 (Test Report/TRACG Input)**

	<b>RPV</b>	<b>Drywell</b>	<b>Wetwell</b>	<b>GDCS</b>	<b>PCC/IC Pools</b>
Total Pressure (bar)	2.36/2.23	2.43/2.23	2.34/2.34	2.35/2.34	0.98/0.98
Air Pressure (bar)(3)	0.0/0.0	0.060/0.054	1.97/2.00	2.21(2)/2.19	N/A
Vapor Temperature (C)	126/123	125/123	72/72	53/54	N/A
Liquid Temperature (C)	126/123	N/A	73/73	53/54	97/97
Collapsed WL (m) (1)	3.8/3/8	0.25/0.0	3.9/3.9	3.4/3.4	4.4/4.4

**Table 2-5****Initial Conditions for PANDA Test P3 (Test Report/TRACG Input)**

	<b>RPV</b>	<b>Drywell</b>	<b>Wetwell</b>	<b>GDCS</b>	<b>PCC/IC Pools</b>
Total Pressure (bar)	1.29/1.29	1.29/1.29	1.30/1.30	1.30/1.30	0.99/0.98
Air Pressure (bar)(3)	0.0/0.0	1.24/1.24	0.81/0.81	1.14 (2)/1.13	N/A
Vapor Temperature (C)	105/107	28/28	79/80	56/56	N/A
Liquid Temperature (C)	105/107	N/A	81/81	N/A	95/95
Collapsed WL (m) (1)	6.1/6.1	0.04/0.0	4.0/4.0	0.07/0.0	4.4/4.4

**Table 2-6****Initial Conditions for PANDA Test P4 (Test Report/TRACG Input)**

	<b>RPV</b>	<b>Drywell</b>	<b>Wetwell</b>	<b>GDCS</b>	<b>PCC/IC Pools</b>
Total Pressure (bar)	2.64/2.43(4)	2.46/2.43	2.34/2.34	2.34/2.34	0.98/0.98
Air Pressure (bar)(3)	0.0/0.0	0.077/0.062	1.94/1.98	2.18(2)/2.18	N/A
Vapor Temperature (C)	128/126	127/126	73/73	56/56	N/A
Liquid Temperature (C)	128/126	N/A	74/74	N/A	98/99
Collapsed WL (m) (1)	12.8/12.8	0.20/0.0	3.9/4.0	0.09/0.0	4.4/4.4

**Table 2-7****Initial Conditions for PANDA Test P5 (Test Report/TRACG Input)**

	<b>RPV</b>	<b>Drywell</b>	<b>Wetwell</b>	<b>GDCS</b>	<b>PCC/IC Pools</b>
Total Pressure (bar)	2.67/2.48(4)	2.52/2.48	2.38/2.39	2.38/2.39	0.98/0.98
Air Pressure (bar)(3)	0.0/0.0	0.077/0.088	1.98/2.04	2.21(2)/2.21	N/A
Vapor Temperature (C)	129/127	126/126	72/72	56/56	N/A
Liquid Temperature (C)	129/127	N/A	72/72	N/A	98/98
Collapsed WL (m) (1)	12.8/12.8	0.15/0.0	4.0/4.0	0.08/0.0	4.6/4.6

**Table 2-8****Initial Conditions for PANDA Test P6 (Test Report/TRACG Input)**

	<b>RPV</b>	<b>Drywell</b>	<b>Wetwell</b>	<b>GDCS</b>	<b>PCC/IC Pools</b>
Total Pressure (bar)	2.56/2.56	2.50/2.47	2.38/2.38	2.37/2.38	1.00/0.98
Air Pressure (bar)(3)	0.0/0.0	0.075/0.071	1.94/2.05	2.20(2)/2.21	N/A
Vapor Temperature (C)	128/128	126/125	71/71	57/57	N/A
Liquid Temperature (C)	128/128	N/A	73/73	N/A	98/98
Collapsed WL (m) (1)	12.6/12.6	0.18/0.0	4.0/4.0	0.08/0.0	4.6/4.6

**Table 2-9****Initial Conditions for PANDA Test P7 (Test Report/TRACG Input)**

	<b>RPV</b>	<b>Drywell</b>	<b>Wetwell</b>	<b>GDCS</b>	<b>PCC/IC Pools</b>
Total Pressure (bar)	2.63/2.63	2.52/2.46	2.39/2.39	2.39/2.39	0.99/0.98
Air Pressure (bar)(3)	0.0/0.0	0.043/0.051	1.96/2.05	2.22(2)/2.22	N/A
Vapor Temperature (C)	129/129	126/126	72/72	57/56	N/A
Liquid Temperature (C)	129/129	N/A	74/74	N/A	97/97
Collapsed WL (m) (1)	12.9/12.9	0.02/0.0	4.0/4.0	0.07/0.0	4.6/4.6

Notes for Tables 2-3 through 2-9

- (1) Vessel water levels are specified relative to the inside bottom elevation.
- (2) GDCS air pressure based on saturated vapor at the GDCS temperature.
- (3) Drywell and wetwell air pressures based on the average of measurements from the available oxygen probes.

**Table 2-10**  
**PCC Instrumentation for PANDA Post-Test Evaluation**

<b>Figure No. (Att. A)</b>	<b>Instrument ID</b>	<b>Measurement</b>
3	MV.P1F	PCC1 inlet flow
3	MV.P2F	PCC2 inlet flow
3	MV.P3F	PCC3 inlet flow
5	ML.U1	PCC1 pool level
5	ML.U2	PCC2 pool level
5	ML.U3	PCC3 pool level
9	MTG.P1.1	PCC1 upper header vapor temperature
10	MTG.P1.2	PCC1 lower header vapor temperature
11	MTG.P2.1	PCC2 upper header vapor temperature
12	MTG.P2.2	PCC2 lower header vapor temperature
13	MTG.P3.1	PCC3 upper header vapor temperature
14	MTG.P3.2	PCC3 lower header vapor temperature
9	MTG.P1.3	PCC1 tube vapor temperature, 0.81m above tube center
9	MTG.P1.4	PCC1 tube vapor temperature, 0.61m above tube center
9	MTG.P1.5	PCC1 tube vapor temperature, 0.41m above tube center
11	MTG.P2.3	PCC2 tube vapor temperature, 0.81m above tube center
11	MTG.P2.4	PCC2 tube vapor temperature, 0.61m above tube center
11	MTG.P2.5	PCC2 tube vapor temperature, 0.41m above tube center
13	MTG.P3.3	PCC3 tube vapor temperature, 0.81m above tube center
13	MTG.P3.4	PCC3 tube vapor temperature, 0.61m above tube center
13	MTG.P3.5	PCC3 tube vapor temperature, 0.41m above tube center
10	MTG.P1.6	PCC1 tube vapor temperature, 0.20m above tube center
10	MTG.P1.7	PCC1 tube vapor temperature at tube center
10	MTG.P1.8	PCC1 tube vapor temperature, 0.41m below tube center
10	MTG.P1.9	PCC1 tube vapor temperature, 0.81m below tube center
12	MTG.P2.6	PCC2 tube vapor temperature, 0.20m above tube center
12	MTG.P2.7	PCC2 tube vapor temperature at tube center
12	MTG.P2.8	PCC2 tube vapor temperature, 0.41m below tube center
12	MTG.P2.9	PCC2 tube vapor temperature, 0.81m below tube center
14	MTG.P3.6	PCC3 tube vapor temperature, 0.20m above tube center
14	MTG.P3.7	PCC3 tube vapor temperature at tube center
14	MTG.P3.8	PCC3 tube vapor temperature, 0.41m below tube center
14	MTG.P3.9	PCC3 tube vapor temperature, 0.81m below tube center

**Table 2-11**  
**DW Instrumentation for PANDA Post-Test Evaluation**

<b>Figure No. (Att. A)</b>	<b>Instrument ID</b>	<b>Measurement</b>
15	MTG.D1.1	DW1 vapor temperature, 7.11m from tank bottom
15	MTG.D1.2	DW1 vapor temperature, 38m from tank bottom
15	MTG.D1.3	DW1 vapor temperature, 4.46m from tank bottom
15	MTG.D1.4	DW1 vapor temperature, 3.13m from tank bottom
15	MTG.D1.5	DW1 vapor temperature, 1.81m from tank bottom
15	MTG.D1.6	DW1 vapor temperature, 0.48m from tank bottom
16	MTG.D2.1	DW2 vapor temperature, 7.11m from tank bottom
16	MTG.D2.2	DW2 vapor temperature, 38m from tank bottom
16	MTG.D2.3	DW2 vapor temperature, 4.46m from tank bottom
16	MTG.D2.4	DW2 vapor temperature, 3.13m from tank bottom
16	MTG.D2.5	DW2 vapor temperature, 1.81m from tank bottom
16	MTG.D2.6	DW2 vapor temperature, 0.48m from tank bottom

**Table 2-12**  
**WW Instrumentation for PANDA Post-Test Evaluation**

<b>Figure No. (Att. A)</b>	<b>Instrument ID</b>	<b>Measurement</b>
17	MTG.S1.1	WW1 vapor temperature, 9.5m from tank bottom
17	MTG.S1.2	WW1 vapor temperature, 8.8m from tank bottom
17	MTG.S1.3	WW1 vapor temperature, 7.6m from tank bottom
17	MTG.S1.4	WW1 vapor temperature, 6.4m from tank bottom
17	MTG.S1.5	WW1 vapor temperature, 5.2m from tank bottom
17	MTG.S1.6	WW1 vapor temperature, 4.0m from tank bottom
19	MTG.S2.1	WW2 vapor temperature, 9.5m from tank bottom
19	MTG.S2.2	WW2 vapor temperature, 8.8 m from tank bottom
19	MTG.S2.3	WW2 vapor temperature, 7.6m from tank bottom
19	MTG.S2.4	WW2 vapor temperature, 6.4m from tank bottom
19	MTG.S2.5	WW2 vapor temperature, 5.2m from tank bottom
19	MTG.S2.6	WW2 vapor temperature, 4.0m from tank bottom
18	MTL.S1.1	WW1 liquid temperature, 3.50m from tank bottom
18	MTL.S1.2	WW1 liquid temperature, 3.20m from tank bottom
18	MTL.S1.3	WW1 liquid temperature, 2.95m from tank bottom
18	MTL.S1.4	WW1 liquid temperature, 2.74m from tank bottom
18	MTL.S1.5	WW1 liquid temperature, 1.99m from tank bottom
18	MTL.S1.6	WW1 liquid temperature, 0.99m from tank bottom
20	MTL.S2.1	WW2 liquid temperature, 3.50m from tank bottom
20	MTL.S2.2	WW2 liquid temperature, 3.20m from tank bottom
20	MTL.S2.3	WW2 liquid temperature, 2.95m from tank bottom
20	MTL.S2.4	WW2 liquid temperature, 2.74m from tank bottom
20	MTL.S2.5	WW2 liquid temperature, 1.99m from tank bottom
20	MTL.S2.6	WW2 liquid temperature, 0.99m from tank bottom
18	MTS.S1.2	WW1 liquid temperature at pool surface
20	MTS.S2.2	WW2 liquid temperature at pool surface

**Table 2-13**  
**Oxygen Probe Instrumentation for PANDA Post-Test Evaluation**

<b>Figure No. (Att. A)</b>	<b>Instrument ID</b>	<b>Measurement</b>
21	MPG.D1.1	DW1 air partial pressure, 6.8m from tank bottom
21	MPG.D1.2	DW1 air partial pressure, 3.1m from tank bottom
21	MPG.D1.3	DW1 air partial pressure, 0.9m from tank bottom
22	MPG.D2.1	DW2 air partial pressure, 6.8m from tank bottom
22	MPG.D2.2	DW2 air partial pressure, 3.1m from tank bottom
22	MPG.D2.3	DW2 air partial pressure, 0.9m from tank bottom

**Table 2-14**  
**IC Instrumentation for PANDA Post-Test Evaluation**

<b>Figure No. (Att. A)</b>	<b>Instrument ID</b>	<b>Measurement</b>
3	MV.IIF	IC inlet flow
5	ML.U0	IC pool level
7	MTG.I1.1	IC upper header vapor temperature
8	MTG.I1.2	IC lower header vapor temperature
7	MTG.I1.3	IC tube vapor temperature, 0.81m above tube center
7	MTG.I1.4	IC tube vapor temperature, 0.61m above tube center
7	MTG.I1.5	IC tube vapor temperature, 0.41m above tube center
8	MTG.I1.6	IC tube vapor temperature, 0.20m above tube center
8	MTG.I1.7	IC tube vapor temperature at tube center
8	MTG.I1.8	IC tube vapor temperature, 0.41m below tube center
8	MTG.I1.9	IC tube vapor temperature, 0.81m below tube center

**Table 2-15**  
**RPV and GDCS Level Instrumentation for PANDA**  
**Post-Test Evaluation**

<b>Figure No. (Att. A)</b>	<b>Instrument ID</b>	<b>Measurement</b>
4	ML.RP.1	RPV collapsed level
4	ML.GD	GDCS level

**Table 2-16**  
**PANDA Measurement Uncertainties**

<b>Measurement</b>	<b>Maximum Uncertainty</b>
Temperature	$\pm 0.8^{\circ}\text{C}$
Pressure	$\pm 2.3 \text{ kPa}$
Flow	$\pm 2\%$
Air Partial Pressure	$\pm 4\%$
PCC/IC Pool Level	$\pm 0.156\text{m}$

**Table 2-17**  
**Assessment of TRACG Accuracy for PANDA Transient (P-Series) Tests**

[

Redacted

]

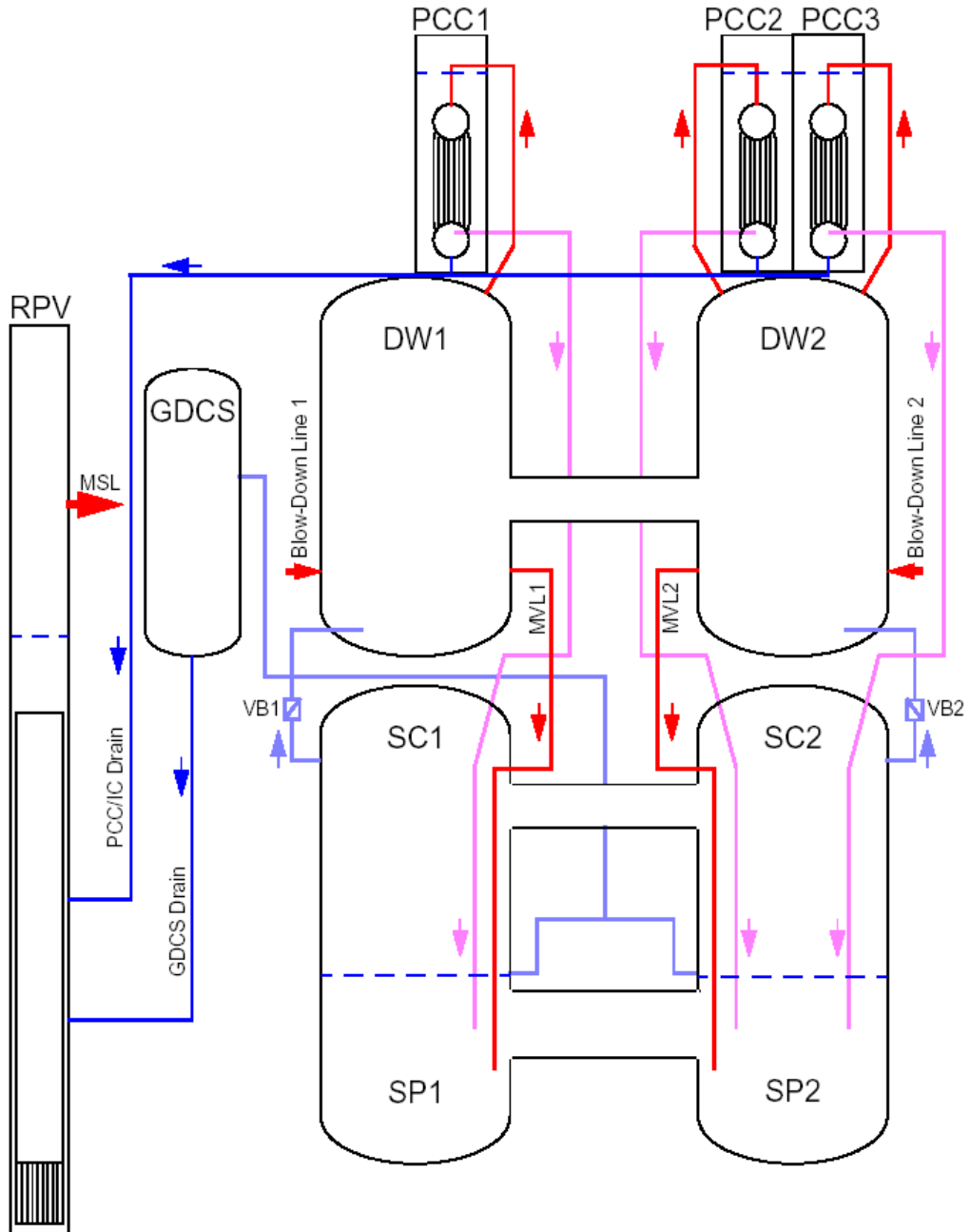


Figure 2-1. PANDA Test Facility Schematic



[

Redacted

]

**Figure 2-2. TRACG Model for ESBWR Long-Term Containment Cooling Transient**

[

Redacted

]

**Figure 2-3. TRACG VSSL Component for PANDA RPV, DW, WW (SC), GDCS and Condenser Pools**

[

Redacted

]

**Figure 2-4. TRACG Model for RPV Riser (TEE09), RPV Heater (CHAN08), and Main Steam Lines (VLVE19 and VLVE20)**

[

Redacted

]

**Figure 2-5. TRACG Models for DW, WW (SC) and SP Connecting Pipes**

[

Redacted

]

**Figure 2-6. TRACG Model for PCCs for Tests with Air as the Only Noncondensable**

[

Redacted

]

**Figure 2-7. TRACG Model for IC**

[

Redacted

]

**Figure 2-8. TRACG Model for PCC Inlet Lines**

[

Redacted

]

**Figure 2-9. TRACG Model for PCC Drain Lines**



[

Redacted

]

**Figure 2-10. TRACG Model for PCC Vent Lines**

[

Redacted

]

**Figure 2-11. TRACG Model for IC Inlet Line**

[

Redacted

]

**Figure 2-12. TRACG Model for IC Drain Line**

[

Redacted

]

**Figure 2-13. TRACG Model for IC Vent Line**

[

Redacted

]

**Figure 2-14. TRACG Model for PCC Drain to IC Drain Connecting Lines**

[

Redacted

]

**Figure 2-15. TRACG PCC Model for Test P7 with Helium**

[

Redacted

]

**Figure 2-16. TRACG Models for Main Vent Lines**

[

Redacted

]

**Figure 2-17. TRACG Model for VB1**



[

Redacted

]

**Figure 2-18. TRACG Model for VB2**

[

Redacted

]

**Figure 2-19. TRACG Model for GDCS Drain Line**

[

Redacted

]

**Figure 2-20. TRACG Model for GDCS to WW Connection Lines**

[

Redacted

]

**Figure 2-21. GDCS, DW, WW (SC) and SP Instrumentation Superimposed on TRACG Nodalization**

[

Redacted

]

**Figure 2-22. PCC1 Instrumentation Superimposed on TRACG Nodalization**

[

**Redacted**

]

**Figure 2-23. IC Instrumentation Superimposed on TRACG Nodalization**

**Attachment A to Section 2**

This attachment contains the figures comparing TRACG calculations to test measurements for the PANDA P-series tests. The figures have been given a special numbering system which utilizes the test number.

Figure P1/8-0. PANDA Facility Configuration for Tests P1 and P8	2A-1
Figure P1/8-1. Drywell and Wetwell Pressures for Test P1/8	2A-2
Figure P1/8-1a. Drywell to Wetwell Pressure Difference for Test P1/8	2A-3
Figure P1/8-2. Measured Heater Power and Calculated PCC Heat Removal for Test P1/8	2A-4
Figure P1/8-3. PCC Inlet Flows for Test P1/8	2A-5
Figure P1/8-5. PCC Pool Levels for Test P1	2A-6
Figure P1/8-9. PCC1 Upper Header and Upper-Tube Gas Temperatures for Test P1/8	2A-7
Figure P1/8-10. PCC1 Lower-Tube and Lower Header Gas Temperatures for Test P1/8	2A-8
Figure P1/8-11. PCC2 Upper Header and Upper-Tube Gas Temperatures for Test P1/8	2A-9
Figure P1/8-12. PCC2 Lower-Tube and Lower Header Gas Temperatures for Test P1/8	2A-10
Figure P1/8-13. PCC3 Upper Header and Upper-Tube Gas Temperatures for Test P1/8	2A-11
Figure P1/8-14. PCC3 Lower-Tube and Lower Header Gas Temperatures for Test P1/8	2A-12
Figure P1/8-15. DW1 Gas Temperatures for Test P1/8	2A-13
Figure P1/8-16. DW2 Gas Temperatures for Test P1/8	2A-14
Figure P1/8-17. WW1 Gas Temperatures for Test P1/8	2A-15
Figure P1/8-18. WW1 Liquid Temperatures for Test P1/8	2A-16
Figure P1/8-19. WW2 Gas Temperatures for Test P1/8	2A-17
Figure P1/8-20. WW2 Liquid Temperatures for Test P1/8	2A-18
Figure P1/8-21. DW1 Air Partial Pressures for Test P1/8	2A-19
Figure P1/8-22. DW2 Air Partial Pressures for Test P1/8	2A-20
Figure P2-0. PANDA Test Facility Configuration for Test P2	2A-21
Figure P2-1. Drywell and Wetwell Pressures for Test P2	2A-22
Figure P2-1a. Drywell to Wetwell Pressure Difference for Test P2	2A-23
Figure P2-2. Measured Heater Power and Calculated PCC Heat Removal for Test P2	2A-24
Figure P2-3. PCC Inlet Flows for Test P2	2A-25
Figure P2-4. RPV and GDCS Collapsed Levels for Test P2	2A-26
Figure P2-5. PCC Pool Levels for Test P2	2A-27
Figure P2-9. PCC1 Upper Header and Upper-Tube Gas Temperatures for Test P2	2A-28
Figure P2-10. PCC1 Lower-Tube and Lower Header Gas Temperatures for Test P2	2A-29
Figure P2-11. PCC2 Upper Header and Upper-Tube Gas Temperatures for Test P2	2A-30
Figure P2-12. PCC2 Lower-Tube and Lower Header Gas Temperatures for Test P2	2A-31
Figure P2-13. PCC3 Upper Header and Upper-Tube Gas Temperatures for Test P2	2A-32
Figure P2-14. PCC3 Lower-Tube and Lower Header Gas Temperatures for Test P2	2A-33
Figure P2-15. DW1 Gas Temperatures for Test P2	2A-34
Figure P2-16. DW2 Gas Temperatures for Test P2	2A-35
Figure P2-17. WW1 Gas Temperatures for Test P2	2A-36
Figure P2-18. WW1 Liquid Temperatures for Test P2	2A-37
Figure P2-19. WW2 Gas Temperatures for Test P2	2A-38
Figure P2-20. WW2 Liquid Temperatures for Test P2	2A-39
Figure P2-21. DW1 Air Partial Pressures for Test P2	2A-40
Figure P2-22. DW2 Air Partial Pressures for Test P2	2A-41
Figure P3-0. PANDA Test Facility Configuration for Test P3	2A-42



Figure P3-1. Drywell and Wetwell Pressures for Test P3	2A-43
Figure P3-1a. Drywell to Wetwell Pressure Difference for Test P3	2A-44
Figure P3-2. Measured Heater Power and Calculated PCC Heat Removal for Test P3	2A-45
Figure P3-3. PCC Inlet Flows for Test P3	2A-46
Figure P3-5. PCC Pool Levels for Test P3	2A-47
Figure P3-11. PCC2 Upper Header and Upper-Tube Gas Temperatures for Test P3	2A-48
Figure P3-12. PCC2 Lower-Tube and Lower Header Gas Temperatures for Test P3	2A-49
Figure P3-13. PCC3 Upper Header and Upper-Tube Gas Temperatures for Test P3	2A-50
Figure P3-14. PCC3 Lower-Tube and Lower Header Gas Temperatures for Test P3	2A-51
Figure P3-15. DW1 Gas Temperatures for Test P3	2A-52
Figure P3-16. DW2 Gas Temperatures for Test P3	2A-53
Figure P3-17. WW1 Gas Temperatures for Test P3	2A-54
Figure P3-18. WW1 Liquid Temperatures for Test P3	2A-55
Figure P3-19. WW2 Gas Temperatures for Test P3	2A-56
Figure P3-20. WW2 Liquid Temperatures for Test P3	2A-57
Figure P3-21. DW1 Air Partial Pressures for Test P3	2A-58
Figure P3-22. DW2 Air Partial Pressures for Test P3	2A-59
Figure P4-0. PANDA Test Facility Configuration for Test P4	2A-60
Figure P4-1. Drywell and Wetwell Pressures for Test	2A-61
Figure P4-1a. Drywell to Wetwell Pressure Difference for Test P4	2A-62
Figure P4-2. Measured Heater Power and Calculated PCC Heat Removal for Test	2A-63
Figure P4-3. PCC Inlet Flows for Test P4	2A-64
Figure P4-5. PCC Pool Levels for Test P4	2A-65
Figure P4-6. DW1 Air Injection Rate for Test P4	2A-66
Figure P4-9. PCC1 Upper Header and Upper-Tube Gas Temperatures for Test P4	2A-67
Figure P4-10. PCC1 Lower-Tube and Lower Header Gas Temperatures for Test P4	2A-68
Figure P4-11. PCC2 Upper Header and Upper-Tube Gas Temperatures for Test P4	2A-69
Figure P4-12. PCC2 Lower-Tube and Lower Header Gas Temperatures for Test P4	2A-70
Figure P4-13. PCC3 Upper Header and Upper-Tube Gas Temperatures for Test P4	2A-71
Figure P4-14. PCC3 Lower-Tube and Lower Header Gas Temperatures for Test P4	2A-72
Figure P4-15. DW1 Gas Temperatures for Test P4	2A-73
Figure P4-16. DW2 Gas Temperatures for Test P4	2A-74
Figure P4-17. WW1 Gas Temperatures for Test P4	2A-75
Figure P4-18. WW1 Liquid Temperatures for Test P4	2A-76
Figure P4-19. WW2 Gas Temperatures for Test P4	2A-77
Figure P4-20. WW2 Liquid Temperatures for Test P4	2A-78
Figure P4-21. DW1 Air Partial Pressures for Test P4	2A-79
Figure P4-22. DW2 Air Partial Pressures for Test P4	2A-80

Figure P5-0. PANDA Test Facility Configuration for Test P5	2A-81
Figure P5-1. Drywell and Wetwell Pressures for Test P5	2A-82
Figure P5-1a. Drywell to Wetwell Pressure Difference for Test P5	2A-83
Figure P5-2. Measured Heater Power and Calculated PCC Heat Removal for Test P5	2A-84
Figure P5-3. PCC Inlet Flows for Test P5	2A-85
Figure P5-5. PCC Pool Levels for Test P5	2A-86
Figure P5-6. DW1 Air Injection Rate for Test P5	2A-87
Figure P5-9. PCC1 Upper Header and Upper-Tube Gas Temperatures for Test P5	2A-88
Figure P5-10. PCC1 Lower-Tube and Lower Header Gas Temperatures for Test P5	2A-89
Figure P5-13. PCC3 Upper Header and Upper-Tube Gas Temperatures for Test P5	2A-90
Figure P5-14. PCC3 Lower-Tube and Lower Header Gas Temperatures for Test P5	2A-91
Figure P5-15. DW1 Gas Temperatures for Test P5	2A-92
Figure P5-16. DW2 Gas Temperatures for Test P5	2A-93
Figure P5-17. WW1 Gas Temperatures for Test P5	2A-94
Figure P5-18. WW1 Liquid Temperatures for Test P5	2A-95
Figure P5-19. WW2 Gas Temperatures for Test P5	2A-96
Figure P5-20. WW2 Liquid Temperatures for Test P5	2A-97
Figure P5-21. DW1 Air Partial Pressures for Test P5	2A-98
Figure P5-22. DW2 Air Partial Pressures for Test P5	2A-99
Figure P6-0. PANDA Test Facility Configuration for Test P6	2A-100
Figure P6-1. Drywell and Wetwell Pressures for Test P6	2A-101
Figure P6-1a. Drywell to Wetwell Pressure Difference for Test P6	2A-102
Figure P6-2. Measured Heater Power and Calculated IC and PCC Heat Removal for Test P6	2A-103
Figure P6-3. IC and PCC Inlet Flows for Test P6	2A-104
Figure P6-5. IC and PCC Pool Levels for Test P6	2A-105
Figure P6-7. IC Upper Header and Upper-Tube Gas Temperatures for Test P6	2A-106
Figure P6-8. IC Lower-Tube and Lower Header Gas Temperatures for Test P6	2A-107
Figure P6-9. PCC1 Upper Header and Upper-Tube Gas Temperatures for Test P6	2A-108
Figure P6-10. PCC1 Lower-Tube and Lower Header Gas Temperatures for Test P6	2A-109
Figure P6-11. PCC2 Upper Header and Upper-Tube Gas Temperatures for Test P6	2A-110
Figure P6-12. PCC2 Lower-Tube and Lower Header Gas Temperatures for Test P6	2A-111
Figure P6-13. PCC3 Upper Header and Upper-Tube Gas Temperatures for Test P6	2A-112
Figure P6-14. PCC3 Lower-Tube and Lower Header Gas Temperatures for Test P6	2A-113
Figure P6-15. DW1 Gas Temperatures for Test P6	2A-114
Figure P6-16. DW2 Gas Temperatures for Test P6	2A-115
Figure P6-17. WW1 Gas Temperatures for Test P6	2A-116
Figure P6-18. WW1 Liquid Temperatures for Test P6	2A-117
Figure P6-19. WW2 Gas Temperatures for Test P6	2A-118
Figure P6-20. WW2 Liquid Temperatures for Test P6	2A-119
Figure P6-21. DW1 Air Partial Pressures for Test P6	2A-120
Figure P6-22. DW2 Air Partial Pressures for Test P6	2A-121
Figure P6-23. VB Leakage Flow Rate for Test P6	2A-122

Figure P7-0. PANDA Test Facility Configuration for Test P7	2A-123
Figure P7-1. Drywell and Wetwell Pressures for Test P7	2A-124
Figure P7-1a. Drywell to Wetwell Pressure Difference for Test P7	2A-125
Figure P7-2. Measured Heater Power and Calculated PCC Heat Removal for Test P7	2A-126
Figure P7-3. PCC Inlet Flows for Test P7	2A-127
Figure P7-5. PCC Pool Levels for Test P7	2A-128
Figure P7-6. DW1 Helium Injection Rate for Test P7	2A-129
Figure P7-11. PCC2 Upper Header and Upper-Tube Gas Temperatures for Test P7	2A-130
Figure P7-12. PCC2 Lower-Tube and Lower Header Gas Temperatures for Test P7	2A-131
Figure P7-13. PCC3 Upper Header and Upper-Tube Gas Temperatures for Test P7	2A-132
Figure P7-14. PCC3 Lower-Tube and Lower Header Gas Temperatures for Test P7	2A-133
Figure P7-15. DW1 Gas Temperatures for Test P7	2A-134
Figure P7-16. DW2 Gas Temperatures for Test P7	2A-135
Figure P7-17. WW1 Gas Temperatures for Test P7	2A-136
Figure P7-18. WW1 Liquid Temperatures for Test P7	2A-137
Figure P7-19. WW2 Gas Temperatures for Test P7	2A-138
Figure P7-20. WW2 Liquid Temperatures for Test P7	2A-139
Figure P7-21. Measured DW1 Air Pressure and Calculated DW1 Air+Helium Pressure for Test P7	2A-140
Figure P7-22. Measured DW2 Air Pressure and Calculated DW2 Air+Helium Pressure for Test P7	2A-141

[

Figures P1/8-0 through P7-22  
(Pages 2A-1 through 2A-141)

Redacted

]

## 3. SIRIUS TWO-PHASE FLOW INSTABILITY TESTS

### 3.1 Introduction

A potential concern during the design of the ESBWR [3-1, 3-2] was the startup process. The design uses a chimney installed on the top of the core to enhance the natural circulation core flow. Experiments have shown that hydraulic oscillations can occur under low pressure and low power conditions during the startup process of a natural-circulation reactor. These hydraulic oscillations include geysering [3-3], flashing-induced instability at low system pressure (0.1 – 0.5 MPa) [3-4], and density wave oscillation at relatively high system pressure (1.0 – 7.2 MPa) [3-5]. In previous studies, TRACG has been successfully qualified against test facility and plant stability data [3-6 and 3-7]. TRACG has also been qualified against geysering data and flashing induced instability data at low system pressure [3-8, 3-9, 3-10]. The study described here was undertaken to provide a qualification basis for the use of TRACG to predict two-phase flow instability at higher pressures.

TRACG analyses were performed to simulate the two-phase flow instability data at relatively high pressure from the SIRIUS loop at the Central Research Institute of the Electric Power Industry (CRIEPI) in Japan. The SIRIUS loop was designed to investigate thermal-hydraulic instabilities in natural-circulation BWRs. In previous qualification studies, TRACG has been qualified against stability data from operating plants and test facilities, including flashing-induced instability data at low pressure from the SIRIUS test facility [3-10]. The TRACG comparisons described here include the dependence of the amplitude and period of the oscillations on heat flux, inlet subcooling and system pressure. Comparisons are also made in terms of stability maps in the plane of inlet subcooling versus heat flux. The objective was to extend the TRACG qualification base for prediction of thermal-hydraulic oscillatory conditions in a natural circulation reactor from startup to normal operation. The evaluation includes a comparison between the nominal operating condition of the ESBWR and the measured stability map at a system pressure of 7.2 MPa to demonstrate the margin to instability in terms of inlet subcooling.

### 3.2 Test Facility and Test Matrix

The SIRIUS test facility was constructed at CRIEPI in Japan to investigate thermal-hydraulic instabilities in BWRs. The test facility was based on non-dimensional scaling of the original SBWR design [3-1] with 70% of the chimney height of the prototype. A schematic of the SIRIUS test facility is shown in Figure 3-1. The test loop consists of two electrically heated channels (1.7-m high), chimney (5.4-m high), separator (upper plenum), downcomer, preheater and subcooler. The total length of the downcomer section is about 30 m. Water temperature at the channel inlet was measured by thermocouples and the flow rate was measured by an orifice flow meter [3-4].

Detailed measurements of the pressure drop across different sections of the test loop under forced liquid flow conditions were previously performed at the SIRIUS test facility in order to obtain local loss coefficients. The test facility is divided into eight regions (see Figure 3-1) and

pressure drops in these locations were measured at different flow rates. Three local loss coefficients were defined as a result of these measurements: loss coefficients for the channel inlet and chimney exit, and loss coefficient for Regions 5 and 6 due to flow merging. These coefficients have been used in the TRACG model.

The transient data for a fixed system pressure were obtained by maintaining constant channel power and adjusting channel inlet subcooling. Channel inlet subcooling was calculated based on system (separator) pressure. For high inlet subcooling, a constant circulation flow was established. By adjusting electrical power to the heater in the preheater, a new channel inlet subcooling was established and corresponding data for pressure drop, flow and temperature were collected. This procedure was then repeated at different channel power levels to generate a stability map in terms of inlet subcooling versus channel power or channel heat flux. The test results showed that the amplitude of flow oscillation changed gradually with the experimental parameters. An unstable condition was judged to have occurred when the standard deviation of the inlet velocity exceeded 10% of the average inlet velocity.

### **3.3 Applicability of Data to ESBWR**

#### **3.3.1 Overview of Data Applicability**

[

Redacted

]

#### **3.3.2 PIRT Phenomena and Coverage**

Data from the CRIEPI Low Pressure Oscillation Tests address the highly ranked PIRT phenomena [3-12] defined below. Additional information on the coverage of these phenomena by the CRIEPI tests is provided in Reference 3-11.

**C12 - Natural Circulation Flow** - Flow from the downcomer to the core and bypass resulting from the difference in the static head outside and inside the shroud region.

**Coverage** - Stable downcomer velocities measured during the CRIEPI tests covered a range of pressure, inlet subcooling and heat flux that is applicable to the ESBWR.

#### **ST1 – Hydrodynamic Stability**

**Coverage** – The tests provide data on the stability of a hydraulic loop that simulates the key ESBWR parameters.

### 3.4 SIRIUS TRACG Input Model and Test Simulation

The TRACG model used for the SIRIUS test facility simulation is shown in Figure 3-2. The nodalization includes two identical channels, a chimney and a separation tank. A TRACG BREK component [3-13] simulates the pressure relief line and provides a constant pressure boundary condition. The downcomer is represented by a combination of one-dimensional PIPE components. The TRACG model was developed based on the test facility drawings with special emphasis on accurate representation of those features of the facility that govern the loop pressure drop and liquid inertia. Experimentally obtained local loss coefficients were incorporated in the TRACG model as described above. The channel inlet subcooling was simulated by changing the outside temperature boundary condition on one of the downcomer pipe components. Comparisons of the differential pressure drop calculated by TRACG to the SIRIUS measurements for the different regions were presented in Reference 3-9. The close agreement between the TRACG results and the data indicates accurate modeling of the channel and chimney regions. The TRACG model includes a detailed representation of the downcomer region that simulates the correct static head and local losses due to fittings and bends.

The TRACG simulation of the SIRIUS test matrix was performed at a system pressure of 2.0 MPa at five power levels: 190, 228, 266, 304, and 457 kW/m<sup>2</sup>, and at a system pressure of 7.2 MPa at three power levels: 609, 761 and 913 kW/m<sup>2</sup>. The TRACG simulations were performed by initially establishing a steady-state condition (stable flow) at high inlet subcooling. Then, by changing the temperature boundary condition, flow regimes at progressively lower inlet subcooling were analyzed. In the absence of specific information on the water level in the separation tank, it was assumed that the water level was the same for all the transient regimes at the prescribed pressure and power conditions.

### 3.5 Results of Post-Test Calculations

#### 3.5.1 Steady-State and Transient Behavior at 2.0 MPa

The stable or steady-state velocity at the channel inlet was calculated as a function of channel inlet subcooling for different heat flux levels and compared with the measurements. Figure 3-3 shows a representative case at a heat flux of 190 kW/m<sup>2</sup>. The agreement between the calculated and measured velocities is within 0.06 m/s (Table 3-1). These results demonstrate that TRACG successfully simulated the characteristics of stable natural circulation flow in the SIRIUS facility in both the single and two-phase regimes.

Figure 3-4 presents transient test results showing the effect of inlet subcooling on the circulation flow at a heat flux of 190 kW/m<sup>2</sup> and inlet subcoolings of 2.5, 14.2, 22.3, 24.3, 30.4 and 37.1 K. At this heat flux level, the test results indicated that there are no flow or void fraction oscillations for channel inlet subcooling greater than 30.4 K or less than 20.4 K. For inlet subcooling between 28.2 and 22.3 K, sinusoidal flow and void fraction oscillations were observed in the test.

Figure 3-5 shows the transient channel inlet velocities calculated by TRACG for the same subcoolings as in Figure 3-4. A visual comparison of Figures 3-4 and 3-5 shows that the subcooling for the onset of oscillatory flow was well predicted and that the calculated velocities are in good agreement with the test data with respect to the effect of inlet subcooling on the amplitude and period of the circulation flow.

Transient results were calculated and compared in detail for low ( $190 \text{ kW/m}^2$ ) and high ( $457 \text{ kW/m}^2$ ) heat fluxes at a system pressure of 2.0 MPa. For the case with heat flux of  $190 \text{ kW/m}^2$  and inlet subcooling of 22.3 K, the measured and calculated inlet velocities and void fractions in Regions 7 and 8 are compared in Figures 3-6 and 3-7, respectively. Figure 3-6 compares the calculated and measured inlet velocities. The calculated period of oscillation is about 1.7 seconds smaller than the measurement (13.5 seconds versus 15.2 seconds). The calculated amplitude (maximum to minimum) is about 0.04 m/s larger than the measurement (0.27 m/s versus 0.23 m/s). Figure 3-7 shows the comparison of average void fractions in Regions 7 and 8. The shape and amplitude of the calculated and measured void fraction oscillations agree well.

For the case with heat flux of  $457 \text{ kW/m}^2$  and inlet subcooling of 48.6 K, the calculated and measured inlet velocities and void fractions in Regions 7 and 8 are compared in Figures 3-8 and 3-9, respectively. Figure 3-8 compares the calculated and measured inlet velocities. The calculated period of oscillation is about 0.7 seconds smaller than the measurement (12.4 seconds versus 11.7 seconds). The calculated amplitude (maximum to minimum) is about 0.10 m/s larger than the measurement (0.79 m/s versus 0.69 m/s). Figure 3-9 shows the comparison of average void fractions in Regions 7 and 8, respectively. The shape and amplitude of oscillations in void fractions agree well between the calculated results and the measurements.

### 3.5.2 Stability Map at 2.0 MPa

For a given heat flux, the channel inlet velocity and channel void fraction are stable for inlet subcoolings below a lower boundary value and above an upper boundary value. For inlet subcoolings between these two boundary values, sinusoidal flow and void fraction oscillations were observed in the test. Figure 3-10 compares calculated and observed upper and lower inlet-subcooling stability boundaries versus heat flux at a pressure of 2.0 MPa. The calculated stability boundaries agree well with the data with respect to both the shape and the trend with heat flux. The calculated lowest heat flux at the cusp of the oscillatory region is  $107 \text{ kW/m}^2$ .

It is of interest to note that the stability boundary predicted by several frequency domain analyses [3-14], for example] leads to the conclusion that there is an unstable region along the zero-quality line toward the origin of Zuber-subcooling plane. The TRACG time domain analysis of the SIRIUS tests showed that this region is stable, in agreement with measurements.

### 3.5.3 Transient Behavior at 7.2 MPa

Figure 3-11 presents transient test results showing the effect of inlet subcooling on the circulation flow at a heat flux of  $760 \text{ kW/m}^2$  with inlet subcoolings of 75.0, 76.7, 90.4 and 94.0 K. Figure 3-12 shows TRACG results for the same heat flux over a range of subcooling from 66.0 to 110.0 K. A visual comparison of Figures 3-11 and 3-12 shows that the calculated results agree well with the test data with respect to the effect of inlet subcooling on circulation flow.



The amplitude of oscillation decreases to near zero when the inlet subcooling is below 66 K and is also significantly reduced when the inlet subcooling is above 110 K.

Observed and calculated transient results at a heat flux of 760 kW/m<sup>2</sup> and an inlet subcooling of 90.4 K are compared in detail in Figures 3-13 and 3-14. Figure 3-13 shows the comparison of observed and calculated channel inlet velocities. In general, the shape of the calculated oscillation is in good agreement with the measurement. The calculated amplitude (maximum to minimum) is about 0.004 m/s smaller than the measurement (0.204 m/s versus 0.208 m/s). Figure 3-14 shows the comparison of observed and calculated average void fractions in Regions 7 and 8. The shape and amplitude of the oscillation in void fraction agree well between the calculated and test results.

### **3.5.4 Stability Map at 7.2 MPa**

Figure 3-15 compares the calculated upper and lower stability boundaries with the test data in terms of channel inlet subcooling versus heat flux at a pressure of 7.2 MPa. The calculated stability boundaries are in reasonable agreement with the data with respect to both the shape and the trend with heat flux. The test results indicate that the flow is stable for heat fluxes less than 609 kW/m<sup>2</sup> at all inlet subcoolings. The calculated lowest heat flux at the cusp of the oscillatory region is 601 kW/m<sup>2</sup>.

### **3.5.5 Comparison of Nominal Operating Conditions to Stability Map**

Typically, BWRs are designed to operate with core inlet subcooling ranging from 10 to 20 K at a system pressure of about 7 MPa. The nominal operating condition of the ESBWR [3-2, 3-15] is shown in Figure 3-15 for comparison to the measured stability map. This figure shows that the ESBWR design has significant inlet subcooling margin of about 50 K to the hydraulic instability region.

## **3.6 Accuracy of TRACG Calculations**

[

Redacted

]

## **3.7 Summary and Conclusions**

TRACG simulations were performed for flow instability tests performed in the CRIEPI SIRIUS facility in Japan. Calculations were performed for system pressures of 2.0 and 7.2 MPa and compared in detail with the corresponding test data. Results of the comparisons show good

agreement between the TRACG results and the data. The key results and conclusion from these comparisons are summarized below.

[

Redacted

]

For cases with sinusoidal oscillations, the shape and amplitude of the oscillations in inlet velocity and void fraction depend on inlet subcooling, heat flux and system pressure. Detailed comparisons between test observations and TRACG calculations were made for cases covering a wide range of inlet subcoolings at low, medium and high heat fluxes and medium and high pressures. The results of these comparisons show that TRACG is capable of predicting the dependence of the oscillation characteristics (amplitude and period) on the relevant system parameters.

[

Redacted

]

The results of these simulations, together with those presented in References 3-8 and 3-9, show that TRACG is capable of predicting thermal-hydraulic instabilities, including geysering, flashing-induced instability at low system pressure and density wave oscillation at relative high system pressure. These qualification studies demonstrate that TRACG can be used to analyze the thermal-hydraulic oscillatory conditions in a natural circulation reactor from start-up to normal operation. Based on comparison of the measured stability map to the ESBWR startup trajectory [3-15] and nominal operating condition (Figure 3-15), the SIRIUS test results support the conclusion that the ESBWR design has significant core inlet subcooling margin to the hydraulic instability region.

### 3.8 References

- 3-1. Upton, H.A., Torbeck, J.E., Billig, P.F., Duncan, J.D., and Herzog, M., *SBWR Design Update: Passively Safe, Nuclear Power Generation for the Twenty First Century*, 4<sup>th</sup> International Conference on Nuclear Engineering (ICONE-4), New Orleans, USA, March 1996.
- 3-2. Cheung, Y.K., Shiralkar, B.S. and Rao, A.S., *Design Evolution of Natural circulation in ESBWR*, 6<sup>th</sup> International Conference on Nuclear Engineering (ICONE-6), San Diego, USA, May 1998.
- 3-3. Aritomi, M., Nakahashi, T., Chiang, J.H., Wataru, M., and Mori, M., *Transient Behavior of Natural Circulation for Boiling Two-phase Flow (Experiment Results)*, 6<sup>th</sup> Proc. Nuclear thermal-hydraulics, ANS 1990 Winter Meeting, Washington, D.C., 313 November 1990.
- 3-4. Inada, F. et al., *Thermal-hydraulic Instability of Natural Circulation BWRs at Low Pressure Start-up; Experimental Estimation of Instability Region with Test Facility Considering Scaling Law*, 3<sup>rd</sup> International Conference on Nuclear Engineering (ICONE-3), Kyoto, Japan, (1995).
- 3-5. Furuya, M. et al., *Two-Phase Flow Instability in a Boiling Natural Circulation Loop at Relatively High System Pressure*, Proc. 8<sup>th</sup> Int. Meeting on Nuclear Reactor Thermal-Hydraulics, Vol. 3, pp. 1778-1784, Kyoto, 1997.
- 3-6. Andersen, J.G.M., et al, *Time-Domain Analysis of Thermal-Hydraulic Stability with TRACG - Sensitivity to Numerical Methods and Qualification to Data*, BWR Stability Symposium, Idaho, (1989).
- 3-7. Andersen, J.G.M., et al., *TRACG Analysis of BWR Plant Stability Data*, Proc. of Int. Workshop on Boiling Water Reactor Stability, OECD, New York, 1990, (1990).
- 3-8. Shiralkar, B.S., et al., *Thermal Hydraulics Aspects of the SBWR Design*, Int. Conf. Des. Safety of Adv. Nucl. Pow. Plants, AESJ, 31,1, (1992).
- 3-9. Andersen, J.G.M. and Klebanov, L.A., *TRACG Analyses of Flashing Instability During Startup-up*, ICONE3, April 1995.
- 3-10. *TRACG Qualification for SBWR*, NEDC-32725P (Rev. 1), August 2002.
- 3-11. *ESBWR Scaling Report*, NEDC-33082P (Rev. 0).
- 3-12. *ESBWR Test and Analysis Program Description*, NEDC-33079 (Rev. 0), August 2002.
- 3-13. Andersen, J.G.M., et al., *TRACG Model Description*, Licensing Topical Report, NEDO-32176 (Rev. 2), March 1996.
- 3-14. Furuya, M., Inada, F. and Yasuo, A., *Thermal-Hydraulic Instability of the Natural Circulation BWR*, 7<sup>th</sup> Report: Analytical Estimation of the Instability at the Higher System Pressure”, Komae Research Laboratory Report Number T95066.
- 3-15. Cheung, Y.K. and Rao, A.S., *Startup Simulation of a Natural Circulation Plant – ESBWR*, ICONE8, March 2000.

**Table 3-1**  
**Assessment of TRACG Accuracy for CRIEPI/SIRIUS Flow Instability Tests**

[

Redacted

]

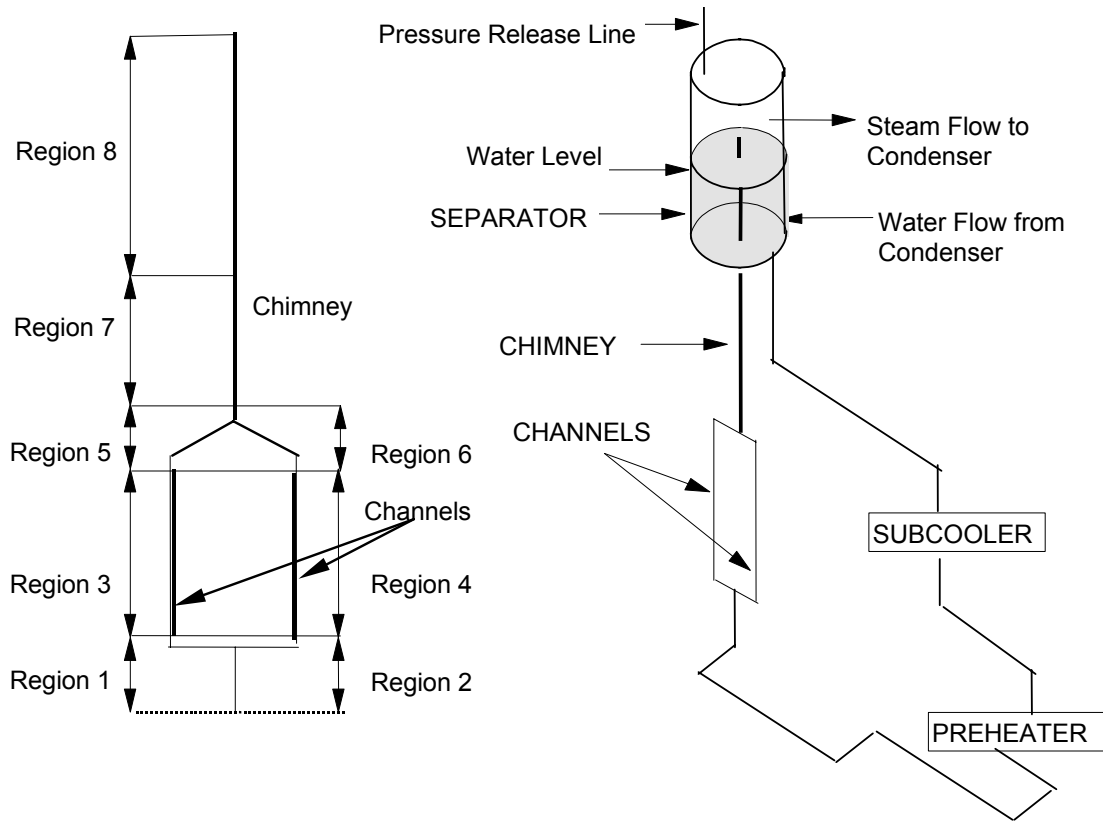


**Figure 3-1. Schematic Diagram of the SIRIUS Thermal Hydraulic Test Facility**

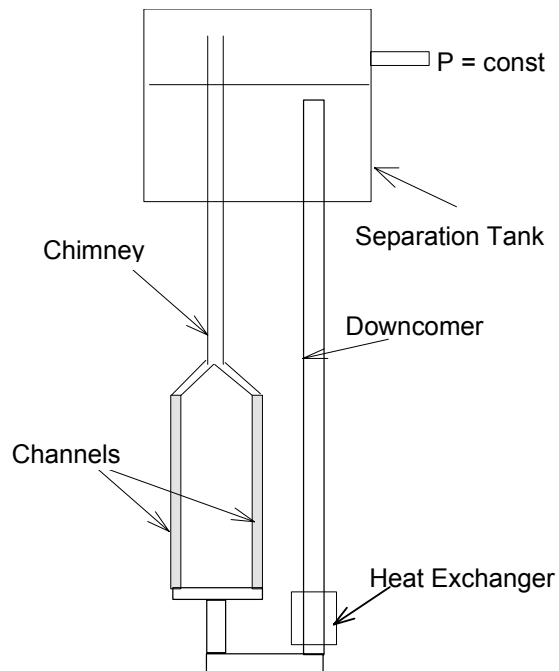


**Figure 3-2. TRACG Model of SIRIUS Test Facility**

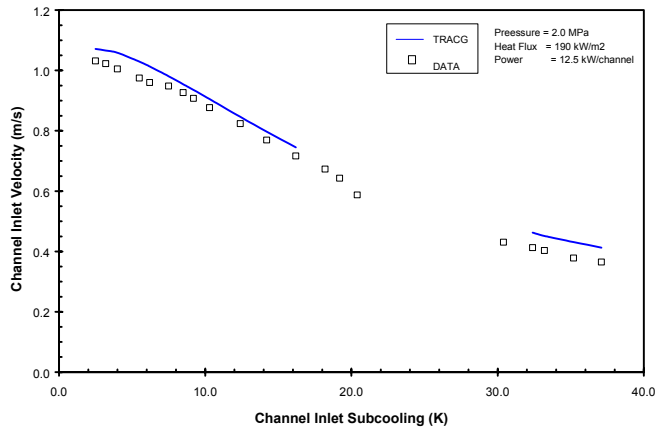


**Figure 3-3. Comparison of Measured and Calculated Steady-State Inlet Velocities as a Function of Inlet Subcooling at 2.0 MPa and 190 kW/ m<sup>2</sup>**

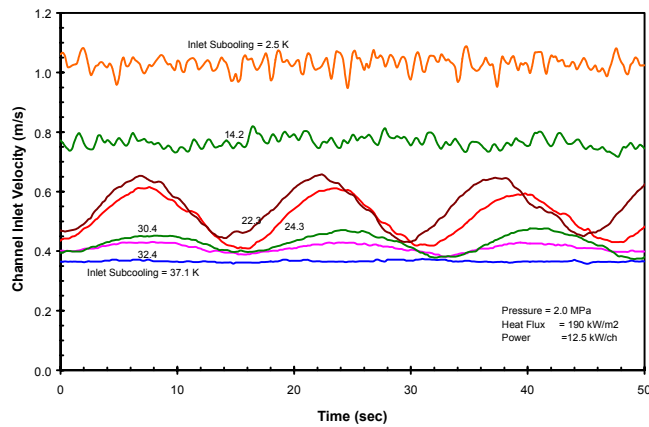


**Figure 3-4. Observed Effect of Inlet Subcooling on Circulation Flow at 2.0 MPa and 190 kW/ m<sup>2</sup>**

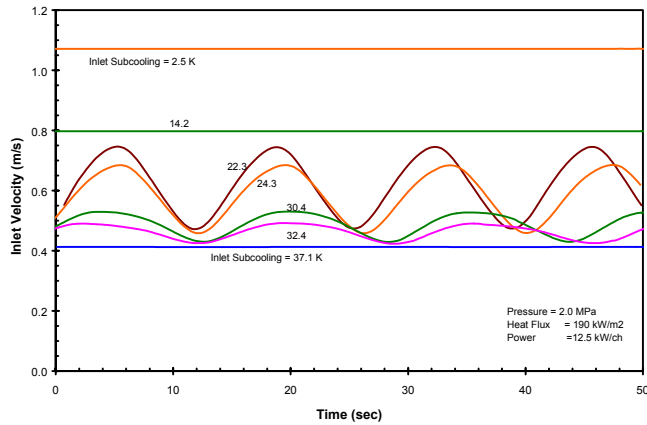


**Figure 3-5. TRACG Calculation of the Effect of Inlet Subcooling on Circulation Flow at 2 MPa and 190 kW/m<sup>2</sup>**

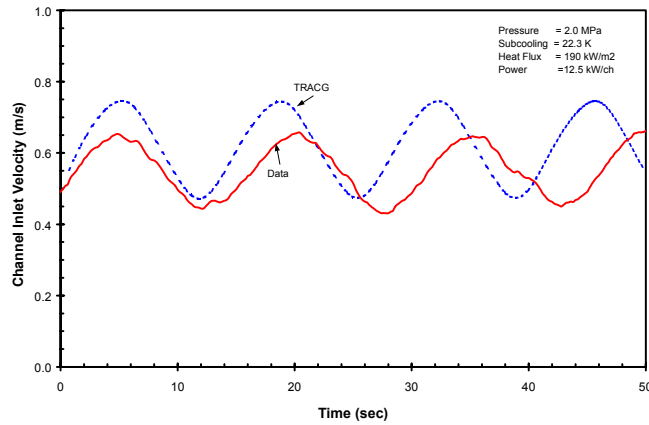
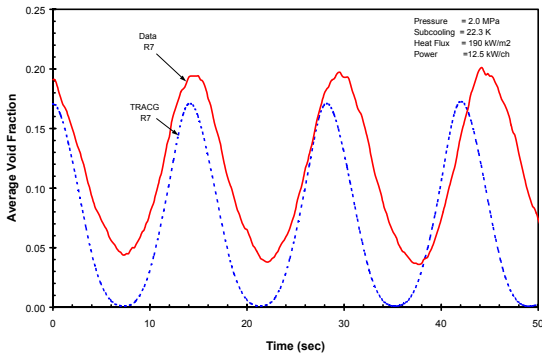
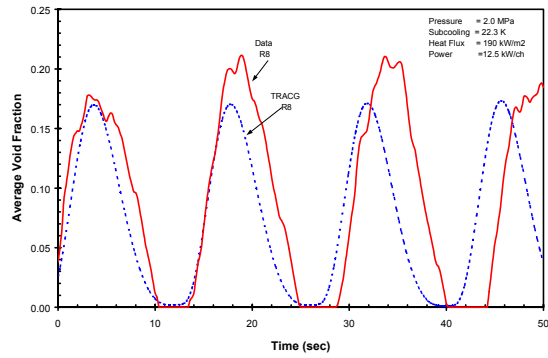


**Figure 3-6. Comparison of Measured and Calculated Channel Inlet Velocity at 2 MPa and 190 kW/m<sup>2</sup> with Inlet Subcooling of 22.3K**



Region 7



Region 8

Figure 3-7. Comparison of Measured and Calculated Average Void Fractions in Regions 7 and 8 at 2 MPa and 190 kW/m<sup>2</sup> with Inlet Subcooling of 22.3 K

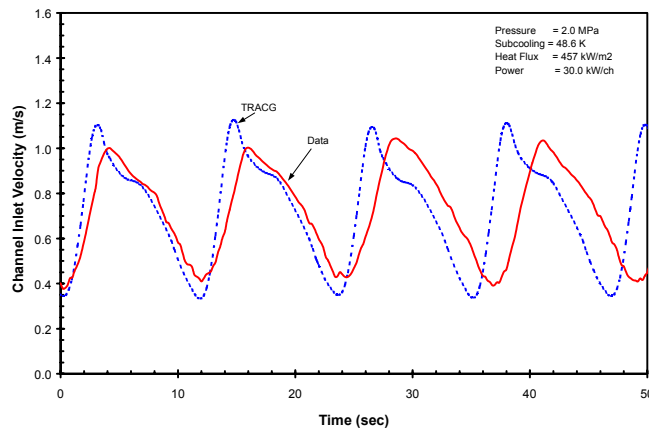
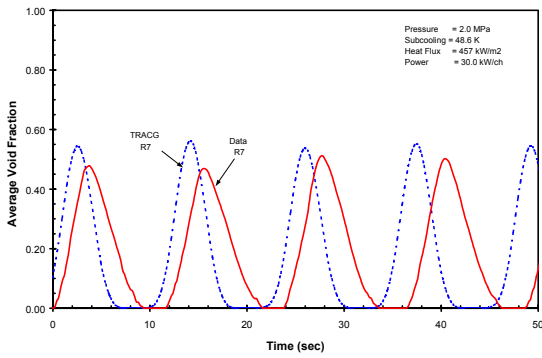
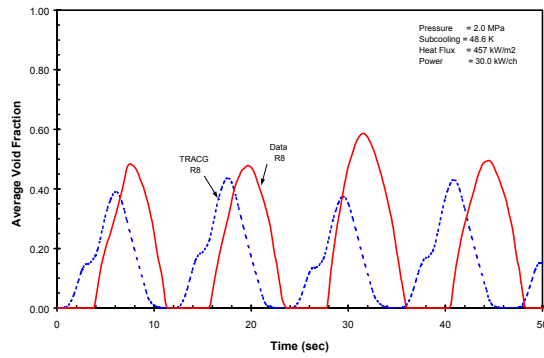


Figure 3-8. Comparison of Measured and Calculated Channel Inlet Velocity at 2 MPa and 457 kW/m<sup>2</sup> with Inlet Subcooling of 48.6 K





Region 7



Region 8

Figure 3-9. Comparison of Measured and Calculated Average Void Fractions in Regions 7 and 8 at 2 MPa and 457 kW/m<sup>2</sup> with Inlet Subcooling of 48.6 K

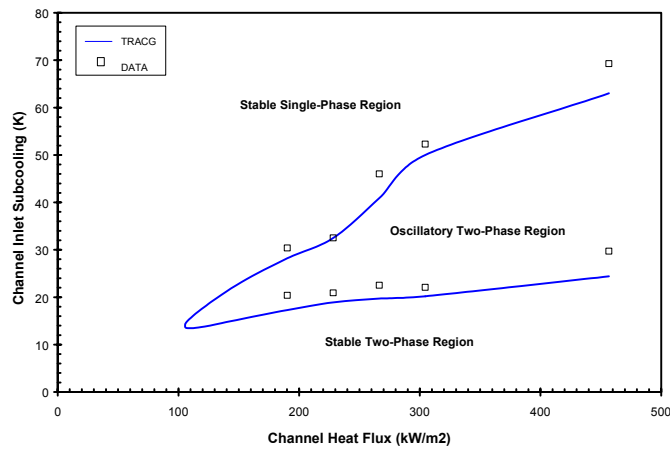
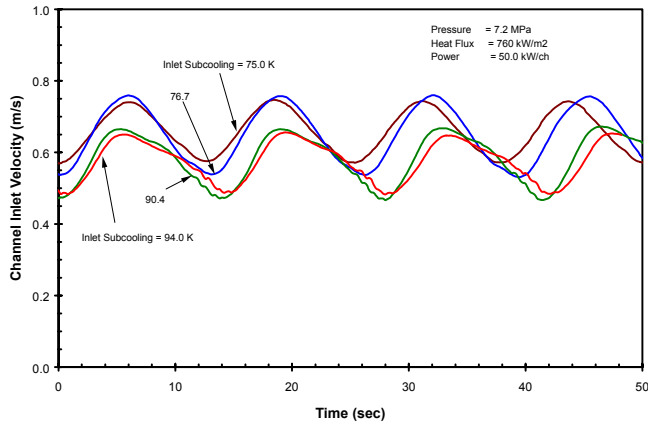
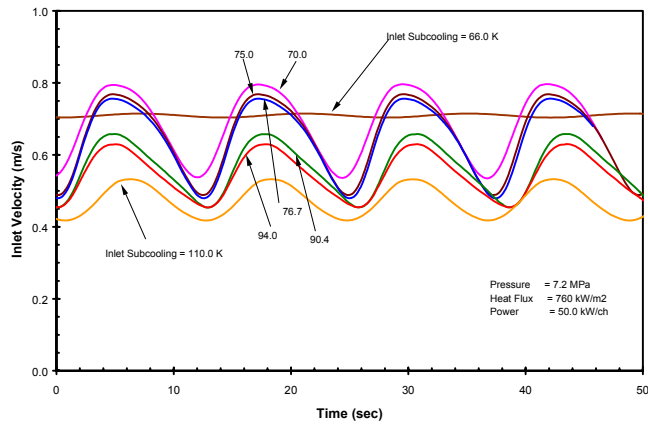


Figure 3-10. Comparison of Calculated and Observed Stability Maps at 2.0 MPa



**Figure 3-11. Observed Effect of Inlet Subcooling on Circulation Flow at 7.2 MPa and 760 kW/ m<sup>2</sup>**



**Figure 3-12. TRACG Calculation of the Effect of Inlet Subcooling on Circulation Flow at 7.2 MPa and 760 kW/m<sup>2</sup>**

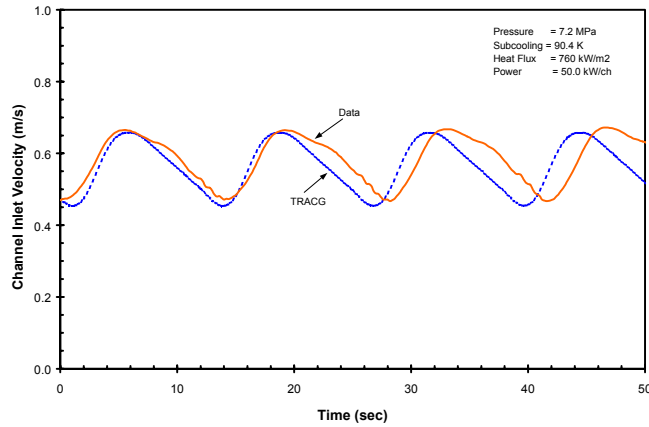


**Figure 3-13. Comparison of Measured and Calculated Channel Inlet Velocity at 7.2 MPa and 760 kW/m<sup>2</sup> with Inlet Subcooling of 90.4**

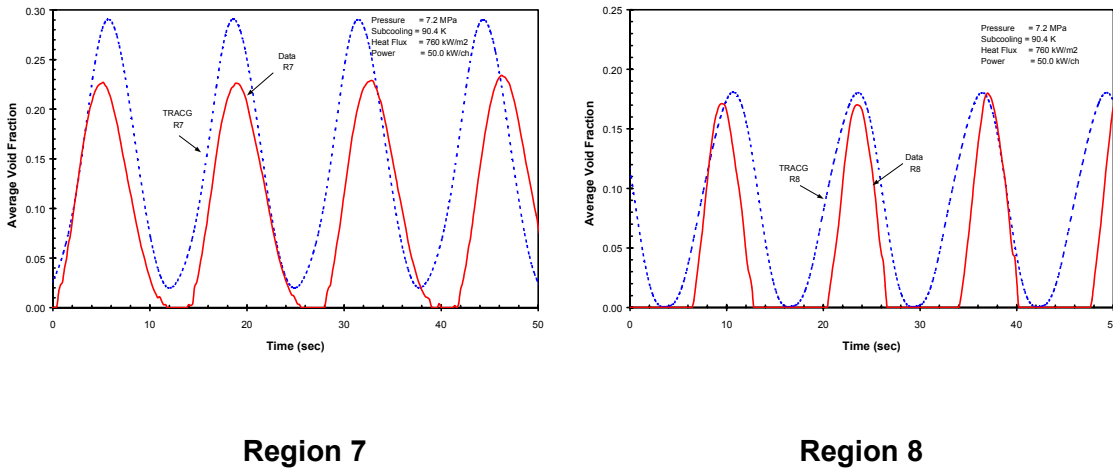


**Figure 3-14. Comparison of Measured and Calculated Average Void Fractions in Regions 7 and 8 at 7.2 MPa and 760 kW/m<sup>2</sup> with Inlet Subcooling of 90.4 K**

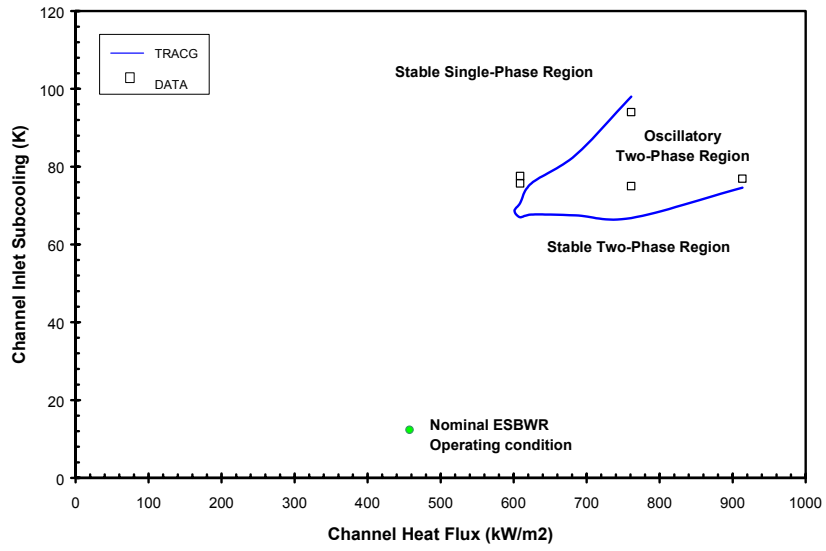


Figure 3-15. Comparison of Calculated and Observed Stability Maps at 7.2 MPa